Research Article

The MBW complex regulates volatiles in petunia flowers: EOBV interacts with AN1 to suppress biosynthesis of phenylpropenes

Oded Skaliter, Raz Cohen, Ehud Leor-Librach, Ekaterina Shor[#], Ori Rudich, Orit Edelbaum, Elena Shklarman, Tania Masci and Alexander Vainstein*

Institute of Plant Sciences and Genetics in Agriculture, The Robert H. Smith Faculty of Agriculture, Food and Environment, The Hebrew University of Jerusalem, Rehovot 7610001, Israel

[#]Present address: Department of Vegetable and Field Crops, Institute of Plant Sciences, Agricultural Research Organization – Volcani Institute, Rishon LeZion 7505101, Israel

***Correspondence: Alexander Vainstein (alexander.vainstein@mail.huji.ac.il)**

The author responsible for distribution of materials integral to the findings presented in this article in accordance with the policy described in the Instructions for Authors (https://academic.oup.com/plphys/pages/General-Instructions) is (Oded Skaliter).

Running title: EOBV is a component of the MBW complex regulating scent

Abstract

Pigment production in petunia is regulated by the bHLH AN1 and the WDR protein AN11, which together with interchangeable MYBs form the MYB–bHLH–WDR (MBW) complex. Pigments and scent are interlinked flower traits, produced via the phenylpropanoid pathway. However, involvement of the MBW complex in regulating floral scent has not been demonstrated. TRV-based suppression of either *AN1* or *AN11* led to an increase in volatile emission, indicating that they are involved in negative regulation of this trait. Yeast two-hybrid and in-planta pairwise and three-way protein–protein interaction assays revealed that EMISSION OF BENZENOIDS V (EOBV) is a component of the MBW complex. Headspace and internal pool analyses of flowers from *eobv*-knockout lines, generated using a viral-based CRISPR/Cas9 system, revealed that EOBV fine-tunes volatile production: phenylpropene levels increased while those of benzenoids and phenylpropanoid-related compounds decreased. Accordingly, transcript levels of *C4H*, directing carbon flux to phenylpropenes, and *ADT3* were significantly elevated in *eobv* flowers, along with decreases in *PAAS* and *BSMT*. *EOBV* is heat-responsive and under a high-temperature regime, in addition to its involvement in scent production, it affected flower development by mitigating reduction of flower size. EOBV's participation in the MBW complex that regulates volatiles and anthocyanins reveals an intriguing molecular link between these showy traits and flower development.

Key words: *Petunia x hybrida*, EOBV, volatiles, CRISPR, MBW complex, heat stress

Introduction

Petunias have evolved distinct sets of showy traits—known as pollination syndromes—to attract their specialized pollinators. These include the production of floral volatiles, such as those emitted by *Petunia axillaris* to attract moths, and pigmentation, with purple flowers in *Petunia inflata* and red ones in *Petunia exserta*, which attract bees and hummingbirds, respectively (Gübitz, T. Hoballah, M.E. Dell'Olivo, A. Kuhlemeier, 2009). Both volatiles and pigments are primarily synthesized from the aromatic amino acid phenylalanine via the phenylpropanoid pathway (Skaliter et al., 2022) through a complex and interlinked network of enzymes and regulators (Fig. 1). The extensive crosstalk between these metabolic branches, yielding phenylalanine-derived volatiles and anthocyanin pigments, has been demonstrated in numerous studies (Zuker et al., 2002; Zvi et al., 2008; Zvi et al., 2012; Cna'ani et al., 2015; Shaipulah et al., 2016; Ravid et al., 2017; Patrick et al., 2021).

The scent bouquet of petunia is comprised of volatiles methyl benzoate, benzaldehyde, benzyl benzoate and benzyl alcohol, which are produced via the C6-C1 (benzenoid) branch following the action of L-PHENYLALANINE AMMONIA LYASE (PAL). In addition, petunia flowers emit C6-C2 volatiles (phenylpropanoid-related compounds) such as phenylethyl alcohol and phenylacetaldehyde, and phenylpropenes (C6–C3) such as eugenol, isoeugenol and vanillin (Fig. 1) (Muhlemann et al., 2014). Production and emission of volatiles are tightly regulated at multiple levels: spatial regulation (Skaliter et al., 2021), physical cellular barriers (Liao et al., 2021; Liao et al., 2023; Skaliter et al., 2024), environmental cues such as ambient temperature and light (Cna'ani et al., 2014; Shor et al., 2023a) and cellular compartmentalization (Cna'ani et al., 2017). Furthermore, involvement of the phytohormones ethylene, gibberellin (GA), auxin and jasmonic acid in the regulation of scent production and emission has been described (Underwood et al., 2005; Liu et al., 2017; Ravid et al., 2017; Lynch et al., 2020; Skaliter et al., 2024). The molecular factors underlying these levels of regulation belong to different families: adenosine triphosphate–binding cassette (ABC) transporters (Adebesin et al., 2017), GRAS (Ravid et al., 2017; Shor et al., 2023a), non-specific lipid transfer proteins (Liao et al., 2023), ethylene-response factors (Liu et al., 2017), basic helix–loop–helix

84 (bHLH) (Shor and Vainstein, 2024) and MADS-box (Bednarczyk et al., 2025). The
85 dominant group of transcriptional regulators of floral volatiles belongs to the MYB
86 superfamily (Verdonk et al., 2005; Spitzer-Rimon et al., 2010; Colquhoun et al., 2011;
87 Spitzer-Rimon et al., 2012; Cna'ani et al., 2015; Skaliter et al., 2024). These regulators
88 bind DNA through their highly conserved N-terminal MYB domain and, depending on
89 their C-terminal domain, can activate or repress target genes (Dubos et al., 2010).
90 EMISSION OF BENZENOIDS I and II (EOBI and EOBII, respectively) and ODORANT1
91 (ODO1) promote the expression of genes encoding enzymes responsible for phenylalanine
92 and dedicated volatiles' biosynthesis, whereas PH4 is required specifically for the
93 volatiles' emission (Verdonk et al., 2005; Spitzer-Rimon et al., 2010; Spitzer-Rimon et al.,
94 2012; Cna'ani et al., 2015). Another MYB activator, EPIDERMIS VOLATILE
95 EMISSION REGULATOR (EVER), is involved in repressing low-vapor-pressure
96 volatiles' emission by modulating the composition of petal epicuticular waxes (Skaliter et
97 al., 2024). The repressor PhMYB4 downregulates transcripts of *CINNAMATE 4-*
98 *HYDROXYLASE* (*C4H*), the enzyme that channels carbon flux to phenylpropenes
99 (Colquhoun et al., 2011). Based on general screening of floral MYBs using virus-induced
100 gene silencing (VIGS) in petunia cv. P720, EOBV has also been suggested as a repressor
101 of volatiles (Spitzer-Rimon et al., 2012), but its mode of action and targets are unknown
102 (Fig. 1).
103 Similar to volatiles, the biosynthesis of anthocyanins is regulated by an intricate
104 network of MYBs. To exert their action, these MYBs interact with bHLH and WD repeat-
105 containing proteins (WDR, also known as WD40) to form the MBW complex
106 (Quattrocchio et al., 1999; Albert et al., 2011; Albert et al., 2014; Zhang et al., 2019). This
107 complex's functionality has been shown to require all members, as mutations in any one
108 of them results in acyanic petals (de Vetten et al., 1997; Quattrocchio et al., 1999; Spelt et
109 al., 2000). In this complex, MYBs provide target-gene specificity, bHLH proteins function
110 as transcriptional co-activators and serve as a physical bridge between MYB and WDR
111 components, and WDR stabilizes the complex and promotes its assembly (Xu et al., 2015;
112 Bulanov et al., 2025). In petunia, the complex typically consists of the bHLH
113 ANTHOCYANIN1 (AN1) and the WDR ANTHOCYANIN11 (AN11), whereas the MYB
114 component that dictates the target and activity of the complex depends on the tissue,

115 environmental conditions or both (Albert et al., 2011; Albert et al., 2014; Zhang et al.,
116 2019). While involvement of the MBW complex in the regulation of phenylpropanoid-
117 derived volatiles' production has not been demonstrated, UNIQUE PLANT
118 PHENYLPROPANOID REGULATOR, a Viridiplantae-specific protein containing a
119 combination of WDR, kinase and RING domains, was recently shown to regulate this
120 process in petunia flowers (Shor et al., 2023b). Moreover, in seeds of sorghum (*Sorghum*
121 *bicolor* L. Moench), a homologous MBW complex was shown to regulate both
122 anthocyanins and fatty acid-derived volatiles (Xie et al., 2019).
123 Here we show involvement of the petunia MBW complex in the regulation of floral
124 volatiles. Using AN1 as bait, we reveal that EOBV is a component of this complex; *eobv*-
125 knockout flowers accumulated higher levels of C6-C3 and lower levels of C6-C1/C2
126 compounds mainly by controlling *C4H* expression. Under high ambient temperatures,
127 flower size and volatile production in eobv-knockout lines were significantly less affected
128 compared to controls, suggesting that EOBV integrates environmental and developmental
129 cues. These results unravel EOBV's mode of action, and by showing its participation in
130 the MBW complex, further demonstrate the interconnection of the regulatory mechanisms
131 underlying the biosynthesis of volatiles and anthocyanins in flowers.
132
133 **Results**
134
135 **VIGS-mediated suppression of *AN1* and *AN11* enhances floral volatile emission in**
136 **petunia**
137
138 Previous studies have shown that core components of the MBW complex, *AN1* and *AN11*,
139 are expressed in young flowers (de Vetten et al., 1997; Spelt et al., 2000). To detail their
140 developmental expression pattern in later stages of flower development, when the volatile
141 machinery is active, RNA was extracted from petal tissues ranging from 4-cm buds to 4
142 days postanthesis (DPA) and analyzed by reverse transcription quantitative PCR (RT-
143 qPCR). Similar to the early stages, *AN1* and *AN11* showed overlapping expression patterns,
144 which aligned with volatile production and emission—peaking at anthesis, remaining high
145 at 1DPA and 2DPA, and declining at 3DPA and 4DPA (Fig. 2a). To evaluate the

146 involvement of the MBW complex in volatile production in petunia, *AN1* and *AN11* were
147 individually suppressed in cv. Mitchell flowers. To achieve this, a 224-bp fragment of
148 *AN1*'s 5' untranslated region (UTR), and 332 bp of the 3' UTR of *AN11*, were amplified
149 from cDNA generated from flowers and cloned into a pTRV2 vector to transiently
150 downregulate their expression using VIGS (Figs. 1a and 1b). Flowers at anthesis were
151 inoculated with *Agrobacterium* carrying pTRV2-AN1, pTRV2-AN11 or pTRV2-
152 CHALCONE SYNTHASE (CHS) as a control (Spitzer et al., 2007), followed by localized
153 headspace sampling (Skaliter et al., 2021). GC–MS analysis revealed a significant increase
154 in emission of the phenylpropenes eugenol and vanillin, the C6-C1 branch compounds
155 benzyl alcohol and methyl benzoate as well as the C6-C2 compound phenylethyl alcohol,
156 in petal tissues inoculated with pTRV2-AN1 and pTRV2-AN11 as compared to control
157 pTRV2-CHS (Fig. 2b). In pTRV2-AN11, emission of (*Z*)-isoeugenol was also enhanced.
158 RT-qPCR analysis (Fig. 2c) and VIGS suppression in anthocyanin-accumulating cv. P720
159 flowers (Fig. S1c) confirmed the suppression activity of the *AN1* and *AN11* constructs.
160 Taken together, these results indicated that while AN1 and AN11 are necessary for
161 anthocyanin biosynthesis, they also negatively affect volatile production.
162
163 **AN1 interacts with the MYB volatile regulator EOBV**
164
165 To identify MYB volatile regulators that may interact with AN1 and AN11, yeast two-
166 hybrid (Y2H) assays were performed. The MYB activators EOBI, EOBII, ODO1 and
167 EVER, and repressors PhMYB4 and EOBV, were tested for interactions. The well-
168 documented interaction between AN1 and AN11 was used as a positive control (Albert et
169 al., 2014). As MYB activators can self-activate the reporter gene *LacZ* when fused to the
170 GAL4 DNA-binding domain (BD), they were fused to the GAL4 activation domain (AD).
171 None of the tested activators interacted with either AN1 or AN11 (Fig. S2). Similarly, there
172 was no interaction between AN1 or AN11 and PhMYB4. In contrast, activation of the
173 target *LacZ* in yeast transformed with EOBV fused to either AD or BD indicated that it
174 interacts with AN1 (Fig. 3a). In line with these results, the signature R/B-like bHLH motif
175 [D/E]Lx2[R/K]x3Lx6Lx3R, which is responsible for interactions of MYBs with bHLH,
176 was identified in the protein sequence of EOBV (Fig. S3) (Zimmermann et al., 2004).

177 Similar to studies on several other MYBs, EOBV did not interact with AN11 when fused
178 to AD or BD (Albert et al., 2014). To further confirm the interaction between EOBV and
179 AN1, in-planta protein–protein interaction assays, using *RUBY* as the reporter gene, were
180 conducted (He et al., 2020; Chen et al., 2023). The assay was based on Chen et al. (2023),
181 except that *RUBY* was placed under the control of six repeats of the lac operator fused to a
182 minimal 35S promoter (6×OpLacI:mini35S), whereas the bait (AN1) was fused to LacI
183 BD, and EOBV and AN11 were each fused to GAL4 AD, all driven by the cauliflower
184 mosaic virus (CaMV) 35S promoter (Fig. S4a). Leaves of *Nicotiana benthamiana* were
185 inoculated with *Agrobacterium* carrying 6×OpLacI:mini35S:*RUBY* together with LacI-
186 AN1 and EOBV-GAL4, or LacI-AN1 and AN11-GAL4 as a positive control, or only LacI-
187 AN1 as a negative control. Betalains were observed in the inoculated tissues 5 days
188 postinoculation, and were extracted and quantified. The analysis revealed accumulation of
189 betalains in LacI-AN1/EOBV-GAL4-inoculated leaves, indicating interaction between the
190 proteins (Fig. 3b). In LacI-AN1/AN11-GAL4-inoculated tissues, betalains accumulated to
191 higher levels than in the LacI-AN1/EOBV-GAL4-inoculated ones, suggesting a stronger
192 interaction. These results are in line with the Y2H assay, which also revealed a stronger
193 interaction between AN1 and AN11 than between AN1 and EOBV. Leaves inoculated only
194 with LacI-AN1 (negative control) showed significantly lower betalain accumulation. To
195 further confirm the interaction between AN1 and EOBV, leaf disks (30 per treatment) of
196 *Nicotiana tabacum* were inoculated with *Agrobacterium* carrying the above constructs and
197 placed on regeneration media. After 2 weeks, inoculated leaf disks were bleached in
198 ethanol and the development of betalain-accumulating calli on the disks was monitored.
199 Multiple pigmented calli were observed on leaf disks inoculated with LacI-AN1/EOBV-
200 GAL4, as well as on those inoculated with LacI-AN1/AN11-GAL4 (Fig. 3c). No
201 pigmented calli were observed on LacI-AN1-inoculated disks. Taken together, the Y2H
202 and in-planta interaction assays demonstrated that EOBV interacts with AN1 of the MBW
203 complex.

204 To test whether EOBV forms a ternary complex with AN1 and AN11, we devised
205 a three-way in-planta protein–protein interaction assay (Fig. S4a). Given the lack of direct
206 interaction between EOBV and AN11 in pairwise assays, we examined whether they can
207 activate 6×OpLacI:mini35S:*RUBY* reporter in the presence of AN1, acting as a bridge to

208 facilitate MBW complex formation. Two new plasmids were generated: p35S:AN1 with
209 pUBQ:DsRed (as a reporter) and p35S:LacI-EOBV (Fig. S4a). *N. benthamiana* leaves
210 were infiltrated with different construct combinations to evaluate the in-planta formation
211 of an active EOBV–AN1–AN11 complex. Co-infiltration of all three components—LacI-
212 EOBV, AN11-GAL4, and AN1—resulted in prominent *RUBY* reporter activation, leading
213 to visible betalain accumulation 48 h postinfiltration (Fig. S4b). In line with these results,
214 betalain extraction and quantification showed that tissues inoculated with LacI-
215 EOBV/AN11-GAL4/AN1 accumulated the highest levels of betalains compared to all
216 other treatments (Fig. 2d). Inoculation of leaves with only two components, LacI-
217 EOBV/AN11-GAL4 or LacI-EOBV/AN1, resulted in significantly lower betalain
218 accumulation, whereas no betalains were detected in tissues inoculated with AN11-
219 GAL4/AN1 or AN1 alone. DsRed expression was observed in all AN1-containing
220 treatments (Fig. S4b). To further confirm the ability of the triad to activate *RUBY*, *N.*
221 *tabacum* disks were inoculated with LacI-EOBV, AN11-GAL4 and AN1 constructs.
222 Pigmented regions were observed in inoculated explants after 2 weeks, demonstrating their
223 ability to activate *RUBY* by forming a complex (Fig.4c). Taken together, these results
224 indicated that EOBV participates in the MBW complex with AN1 and AN11.
225
226 **EOBV is a petal-specific repressor that belongs to MYB family subgroup 4**
227
228 To characterize the evolutionary relationship of EOBV in the MYB family, we performed
229 a phylogenetic analysis of MYBs from various plant species. Phylogenetic analysis
230 clustered EOBV into MYB family subgroup 4 (Dubos et al., 2010), which contains
231 previously characterized MYB repressors (Figs. 4a and S5) (Ma and Constabel, 2019).
232 More specifically, EOBV clustered in the SG4-AtMYB subclass together with MYBs
233 regulating phenylpropanoid biosynthesis (Jin et al., 2000; Colquhoun et al., 2011; Zhang
234 et al., 2023). Its closest homolog was tomato (*Solanum lycopersicum*) MYB7, shown to be
235 involved in negative regulation of anthocyanins (Zhang et al., 2023). InterPro analysis
236 (Blum et al., 2021) of EOBV revealed that similar to most subgroup 4 members, EOBV
237 has two conserved motifs at its C terminus: C1 (LlsrGIDPxT/sHRxI/L) and C2
238 (pdLNLD/ELxiG/S), the latter part of the ethylene-responsive element binding factor-

239 associated amphiphilic repression (EAR) motif which is responsible for the repression
240 activity (Fig. S3) (Ohta et al., 2001; Chen et al., 2019). EOBV also has a zinc-finger domain
241 C3 motif ($CX_{1-2}CX_{7-12}CX_2C$) and a C4 motif (FLGLx4-7V/LLD/GF/YR/Sx1LEMK),
242 which is typical for the SG4-AtMYB subclass (Fig. S3) (Chen et al., 2019). To determine
243 whether, like most MYBs, EOBV is located in the nucleus, it was fused to green fluorescent
244 protein (GFP) at either the N or C terminus and transiently expressed in petunia petals.
245 Confocal microscopy confirmed that the GFP signal of EOBV-GFP and GFP-EOBV co-
246 localizes with a red fluorescent protein (RFP) fused to a nuclear localization signal (NLS),
247 which served as a positive control for nuclear localization (Fig. 4b).
248 To detail the spatial expression profile of *EOBV*, RT-qPCR was performed on RNA
249 extracted from various vegetative and floral tissues. *EOBV*'s expression was found to be
250 petal-specific, with transcript levels in the other tissues—androecium, gynoecium, sepals,
251 roots, shoots and leaves—at substantially lower or background levels (Fig. 4c).
252 Furthermore, analysis of the petunia petal adaxial epidermis transcriptome (Skaliter et al.,
253 2024)—the main site of volatile emission (Skaliter et al., 2021)—revealed enrichment of
254 *EOBV* transcript, with approximately 1.8-fold higher expression than in the whole petal
255 (Fig. 4d). Analysis of the petal transcriptome (Shor et al., 2023b) from petunia buds and
256 1DPA flowers, in the morning vs. evening, revealed highest *EOBV* expression in flowers
257 during the evening (Fig. S6). Its diurnal pattern changed according to developmental stage:
258 higher in the morning vs. evening in buds and vice versa in 1DPA flowers.
259
260 **TRV-based suppression of *EOBV* in petunia flowers alters volatile composition**
261
262 To evaluate EOBV's effect on volatiles, a 164-bp fragment of its 3' UTR was amplified
263 and cloned into pTRV2 (Fig. S7a). 'Mitchell' flowers at anthesis were inoculated with
264 *Agrobacterium* carrying either TRV2-EOBV or TRV2-CHS. Localized headspace analysis
265 revealed a significant increase in the phenylpropenes eugenol and (*Z*)-isoeugenol, with a
266 concomitant decrease in emission of methyl benzoate and phenylacetaldehyde in TRV2-
267 EOBV-inoculated tissues (Fig. 4e). RT-qPCR analysis confirmed that *EOBV* transcripts
268 were reduced by ca. 60% in these tissues compared to control TRV2-CHS. To test whether
269 EOBV is involved in anthocyanin regulation, plants of petunia cv. Classic Blue Ray,

270 producing purple-pigmented flowers, were inoculated with the aforementioned TRV2
271 vectors. Extraction of total anthocyanins from flowers of plants inoculated with TRV2-
272 EOBV revealed that, in contrast to its homolog in tomato, suppression of *EOBV* does not
273 affect anthocyanin content (Fig. S7b). GA has been shown to repress volatile and induce
274 anthocyanin production in petunia flowers (Ravid et al., 2017). To determine GA's effect
275 on *EOBV* expression, 4-cm buds were treated with exogenous GA_3, followed by RT-qPCR
276 analysis. Transcript levels of *GIBBERELLIN-INDUCED PROTEIN 2*, used as a positive
277 control for GA application, increased following GA treatment (Fig. S8) (Ben-Nissan et al.,
278 2004; Skaliter et al., 2024). In line with the observed lack of EOBV effect on anthocyanin
279 levels, its transcript level was unaffected by GA_3 application, suggesting that *EOBV* is not
280 regulated by GA.
281
282 **EOBV controls phenylpropene production through transcriptional suppression of**
283 ***C4H***
284
285 To detail EOBV's involvement in the regulation of volatiles production and emission,
286 knockout mutations were induced in petunia cv. Mitchell using the viral-based
287 CRISPR/Cas9 system (Skaliter et al., 2024). The petunia genome has a single copy of
288 *EOBV* that is comprised of two exons and one intron (Fig. 5a) (Bombarely et al., 2016).
289 Three spacers targeting exon 1, including one directly targeting the start codon, were
290 designed using the CRISPOR tool (Concordet and Haeussler, 2018) (Fig. 5a). To generate
291 vectors with two spacers each, single guide RNA with spacer 1 (sgRNA1) was cloned into
292 pTRV2 vectors together with either sgRNA2 or sgRNA3 (Fig. 5b). *Cas9*-expressing
293 explants (Skaliter et al., 2024) were inoculated with *Agrobacterium* harboring either
294 pTRV2-*sgRNA1*-*sgRNA2* or pTRV2-*sgRNA1*-*sgRNA3* (Fig. 5b). Three independent T2
295 homozygous *eobv*-knockout lines were selected for further analyses: *eobv*-#1 with a 128-
296 bp deletion between the target sites of spacers 1 and 2; *eobv*-#2 harboring two thiamine
297 insertions, one at the spacer 1 target site and one at the spacer 2 target site; and *eobv* -#3
298 with a thiamine insertion at the spacer 1 (2 bp upstream of the start codon) target site and
299 a thiamine deletion at the spacer 3 target site (Fig. 5b). In *eobv*-#1, the start codon was
300 deleted together with the first 42 amino acids, and in lines *eobv*-#2 and #3, the mutations

301 led to premature stop codons after 58 and 91 amino acids, respectively (Fig. 5c). Plants of
302 the three *eobv*-knockout lines developed and flowered normally (Fig. 5d).
303 To evaluate the effect of *eobv* knockout on the emission levels of volatiles, dynamic
304 headspace analyses were conducted on flowers of *eobv*-knockout lines and control *Cas9*.
305 In agreement with the VIGS experiment, emission levels of the C6-C3 branch compounds
306 vanillin, eugenol and isoeugenol isomers significantly increased in *eobv*-knockout lines
307 compared to control *Cas9*-expressing plants (Fig. 6a). In contrast, emission levels of all
308 C6-C1/C2 compounds were significantly reduced in *eobv*-knockout lines, excluding benzyl
309 benzoate, leading to a decrease in total emission levels in these lines (Fig. 6a). To examine
310 whether *eobv* knockout affects the production of volatiles, internal pools were analyzed in
311 flowers of the mutant lines and compared to control *Cas9* plants. In agreement with the
312 headspace results, compounds generated via the phenylpropene branch (C6-C3)—
313 isoeugenol isomers, eugenol and vanillin—significantly increased in *eobv* lines compared
314 to control *Cas9* flowers (Fig. 6b). Levels of methyl benzoate, benzaldehyde, benzyl
315 benzoate and benzyl alcohol (C6-C1) and phenylethyl alcohol and phenylacetaldehyde
316 (C6-C2) were not affected by *eobv* knockout (Fig. 6b). Taken together, these results
317 indicated that EOBV is a negative regulator of phenylpropene production and emission.
318 To gain a deeper understanding of EOBV's mode of action, transcript levels of
319 genes encoding key biosynthesis enzymes and transcriptional regulators of volatile
320 production were analyzed by RT-qPCR in *eobv*-knockout lines. Most of the tested genes,
321 such as *ODO1*, *EOBI*, *EOBII*, *PhMYB4*, *EVER*, *PHENYLPROPANOID EMISSION-*
322 *REGULATING SCARECROW-LIKE (PES)*, *PhDEFICIENS (PhDEF)* and *PAL1* and *2*,
323 showed no differences in transcript levels between flowers of *eobv*-knockout lines and
324 control *Cas9* (Fig. 7). Similarly, despite the observation that MYBs participating in the
325 MBW complex can affect the expression of their counterparts—e.g., *AN1* expression is
326 enhanced in leaves ectopically expressing *AN2* and in *MYB27*-RNAi lines (Spelt et al.,
327 2000; Albert et al., 2014), transcripts levels of *AN1* and *AN11* were unaltered in *eobv* lines.
328 Concordant with the decreased emission of phenylacetaldehyde, phenylethyl alcohol and
329 methyl benzoate, *PHENYLACETALDEHYDE SYNTHASE* (*PAAS*) and *S-ADENOSYL-L-*
330 *METHIONINE:BENZOIC ACID/SALICYLIC ACID CARBOXYL*
331 *METHYLTRANSFERASE* (*BSMT*) transcript levels decreased in the knockout lines (Fig.

332 6). Moreover, transcript levels of *C4H2*, which controls carbon flux to the C6-C3 branch,
333 were significantly elevated in *eobv*-knockout lines, corresponding to the increase in
334 emission and pools of compounds derived from that branch (Figs. 6a, 6b and 7). Transcript
335 levels of *EOBV* were unaltered in the *eobv* lines. AtMYB4, an *Arabidopsis* homolog of
336 EOBV, has been shown to repress its own promoter, hence knockout of *eobv* may lead to
337 a break in a negative feedback loop (Zhao et al., 2007). Furthermore, the system's ability
338 to recognize aberrant mRNAs is highly complex and requires multiple factors to trigger
339 RNA degradation via nonsense-mediated mRNA decay (Luha et al., 2024).

340 The promoter of *C4H2* contains two repeats of the MYB binding motif
341 YACCWACY at nucleotide positions –115 and –205. AtMYB4 has been shown to bind to
342 this motif in promoter regions proximal to the transcription start site (Agarwal et al., 2020).
343 In contrast to *C4H2*, *PAAS* and *BSMT* promoters do not contain this motif (Fig. S9a). To
344 identify additional potential targets of EOBV, in-house Python-based motif scanning of the
345 petunia genome was performed, as bioinformatic tools such as MEME (meme-suite.org)
346 do not include a petunia database. To this end, 300-bp sequences from all annotated genes
347 in the *P. axillaris* genome (Bombarely et al., 2016) were extracted and scanned for the
348 motif YACCWACY (e value ≤ 0.005). Genes with low or no expression in the petunia
349 petal transcriptome (Shor et al., 2023b) or lacking annotation were excluded. Moreover, as
350 multiple motifs are often required for efficient regulation of target genes, as also evident
351 from the two copies present in the *C4H2* promoter, only sequences containing two or more
352 copies of the motif were included (Espley et al., 2009); 39 candidate genes were identified.
353 According to predicted annotations, these candidates are involved in lignin and
354 phenylpropanoid biosynthesis, cell wall remodeling and expansion, hormonal signaling,
355 and secondary metabolism, integrating structural, developmental, flowering and stress-
356 related processes, and representing a broad range of processes potentially involving EOBV
357 (Table S1). Among the genes involved in phenylpropanoid biosynthesis was another copy
358 of *C4H* in petunia—*C4H1*, whose expression is much lower in petunia flowers when the
359 scent machinery is active compared to that of *C4H2* (Colquhoun et al., 2011). In addition,
360 two genes involved in aromatic amino acid biosynthesis were identified: *CHORISMATE*
361 *SYNTHASE (CS)* responsible for conversion of 5-enolpyruvylshikimate-3-phosphate to
362 chorismate and *AROGENATE DEHYDRATASE 3* (*ADT3*), which converts arogenate to

363 phenylalanine, the main precursor of phenylpropanoids. To determine whether EOBV
364 regulates these genes, their expression was analyzed in *eobv* flowers by RT-qPCR.
365 Transcript levels of *ADT3* were significantly higher in *eobv* compared to control *Cas9*
366 flowers (Fig. S9b). In contrast, transcripts of *C4H1* and *CS* were unaltered in the *eobv*
367 flowers. These findings indicated that EOBV regulates genes encoding enzymes involved
368 in both the synthesis of phenylpropanoid precursors and the downstream steps of the
369 phenylpropanoid pathway.
370 The phenotypes observed in the *eobv*-knockout lines, i.e., increased emission of
371 phenylpropenes with concomitant decrease in benzenoids and elevated levels of *C4H2*,
372 resemble the effect reported by Colquhoun et al. (2011) for RNAi-mediated suppression of
373 *PhMYB4*. However, although the diel pattern was similar, the spatial developmental pattern
374 was different: in contrast to EOBV, *PhMYB4* was not enriched in the adaxial epidermis
375 (Fig. S10). Moreover, in the *eobv*-knockout lines, *PhMYB4* transcript levels were similar
376 to those in the *Cas9* control, indicating that EOBV does not affect *PhMYB4* expression
377 (Fig. 7). Although off-target gene-editing events induced by Cas9 in plants are generally
378 considered to be rare, they have been reported to occur at genomic sites with high sequence
379 similarity to the target (Sturme et al., 2022). Considering a nucleotide identity between
380 *EOBV* and *PhMYB4* of 80.34% (mRNA), the three spacers selected to target *EOBV*
381 contained 4 to 10 mismatches relative to *PhMYB4*, including 2 to 5 mismatches within the
382 critical seed sequence, to lower the chances of off-target gene editing (Fig. S11a). Sanger
383 sequencing of *PhMYB4* in *eobv*-knockout lines confirmed that no editing events had
384 occurred in *PhMYB4*'s sequences in those lines (Fig. S11b). Taken together, these results
385 indicated that the phenotype of *eobv*-knockout lines is not dependent on PhMYB4.
386
387 **Stacking of *ever*- and *eobv*-knockout alleles has no additive effect on phenylpropene**
388 **emission in petunia flowers**
389
390 Given their major relevance in the ornamental, agricultural, food and beverage, and
391 pharmaceutical industries, enhanced production of phenylpropene volatile compounds is a
392 biotechnological goal (Skaliter et al., 2022). We previously identified EVER, a MYB
393 transactivator that regulates the emission of low-vapor-pressure volatiles, e.g.,

394 phenylpropenes, by modulating the composition of petal epicuticular waxes (Skaliter et al.,
395 2024). Because EVER and EOBV influence phenylpropene levels through distinct
396 mechanisms—modification of the epicuticular wax layer (Fig. 1) and suppression of *C4H2*
397 and *ADT3*, respectively—we tested whether generating petunia flowers with double
398 knockouts of *ever* and *eobv* would result in an additive increase in phenylpropene emission;
399 *ever* line #2, which exhibited an increase of ca. 1.7-fold in emission levels of
400 phenylpropenes (Skaliter et al., 2024), and *eobv* line #1 were cross-pollinated to produce
401 F1 hybrids that were subsequently self-pollinated until an F3 population with homozygous
402 knockout mutations was generated. F3 plants and flowers of *ever* x *eobv* developed
403 normally and did not differ from *eobv*, *ever* or control *Cas9* (Fig. S12a). Headspace
404 analysis revealed that flowers of *ever* x *eobv* had higher levels of phenylpropenes than the
405 control *Cas9*; however, none of the volatiles were at higher levels than in the parental lines
406 *eobv* and *ever* (Fig. S12b), suggesting limited carbon availability for phenylpropanoid
407 volatile production.
408
409 **Knockout of *eobv* mitigates the effect of high ambient temperature on floral traits**
410
411 *EOBV* transcripts are heat-responsive, their levels significantly increasing in flowers of
412 petunia cvs. P720 and Blue Spark grown at high ambient temperature (Cna'ani et al., 2014).
413 To detail the involvement of EOBV in regulating volatiles under high ambient temperature,
414 plants of *eobv*-knockout lines and control *Cas9* were first grown under standard growth
415 conditions (22/16°C day/night) and then half were transferred to a higher temperature
416 regime (28/22°C day/night). In line with Sood et al. (2021), the control flowers were
417 significantly affected (~12% smaller in diameter) by the high ambient temperature (Fig.
418 8a). As expected, there was no difference in diameter between flowers of *Cas9* and *eobv*
419 at 22/16°C (Figs. 5d and 8a). High temperature had a less pronounced effect on flower size
420 of the *eobv* plants (6% reduction) and their diameter remained higher than those of *Cas9*
421 plants grown at 28/22°C (Fig. 8a). RT-qPCR analysis targeting *EOBV* transcripts revealed
422 an increased level in flowers of *Cas9* plants grown at higher ambient temperature,
423 confirming that *EOBV* is also heat-responsive in the 'Mitchell' genomic background (Fig.
424 8b). *EOBV* transcript levels were unaltered in *eobv* knockouts at elevated temperature,

425 indicating that the multicomplex machinery regulating accumulation of transcripts does not
426 recognize aberrant *eobv* mRNA under both standard and heat-stress conditions. To assess
427 whether the difference in petal size observed under elevated temperatures is associated with
428 changes in α-expansin (PhEXP1), shown to be involved in regulation of petal size (Zenoni
429 et al., 2004), its transcript levels were quantified in *Cas9* and *eobv* flowers grown at
430 22/16°C and 28/22°C. *PhEXP1* expression was significantly reduced at 28°C in both
431 genotypes to a similar extent, indicating that its downregulation under heat conditions
432 occurs independently of EOBV (Fig. S13).

433 Analysis of expression levels of EOBV's target, *C4H2*, revealed that it is
434 significantly reduced in response to high temperature in both *Cas9* and *eobv* flowers (Fig.
435 8b). Moreover, transcript levels of *PhMYB4*, which also regulates *C4H2*, decreased
436 slightly, albeit not significantly, at higher ambient temperatures in both *eobv* and *Cas9*
437 (Fig. S13). Expression levels of *ADT3*, the other target of EOBV, were only mildly affected
438 by heat stress, showing a non-significant decline in *Cas9* flowers grown at 28/22°C
439 compared to 22/16°C. In *eobv* lines, *ADT3* transcript levels decreased significantly under
440 elevated temperature, reaching levels comparable to those in *Cas9* flowers. Dynamic
441 headspace analysis of *eobv* and *Cas9* flowers revealed that, consistent with Cna'ani et al.
442 (2015), total volatiles in *Cas9* at 28/22°C are significantly reduced, owing to the decrease
443 in the major emitted compounds—benzaldehyde, benzyl alcohol and methyl benzoate (Fig.
444 8c). In *eobv* flowers, total emission levels were not significantly altered, because levels of
445 methyl benzoate decreased, benzyl alcohol levels remained unchanged, and benzaldehyde
446 levels increased. Interestingly, the emission levels of phenylacetaldehyde were
447 significantly increased at 28/22°C in both *Cas9* and *eobv* lines. None of the
448 phenylpropenes' levels were affected by high ambient temperature in *Cas9* flowers,
449 whereas isoeugenol isomers in *eobv* declined significantly, revealing that carbon flux under
450 high temperature is affected by EOBV but probably not via C4H2 or ADT3.

451

452 **Discussion**

453

454 Specialized metabolite biosynthesis is not confined to individual pathway branches
455 but occurs through interconnected activity across multiple metabolic layers. For example,

456 increasing flux through the phenylpropanoid pathway led to enhanced terpenoid
457 biosynthesis, and vice versa (Zvi et al., 2012; Skaliter et al., 2026). At the inter-pathway
458 level of phenylpropanoid metabolism, anthocyanin and volatile biosynthesis are tightly
459 interlinked, as shifting metabolic flux toward either branch can enhance production in the
460 other, and in some cases, increased flux leads to simultaneous enhancement of both
461 branches (Zuker et al., 2002; Zvi et al., 2008; Zvi et al., 2012; Cna'ani et al., 2014; Cna'ani
462 et al., 2015; Shaipulah et al., 2016; Ravid et al., 2017). Conversely, high ambient
463 temperatures lead to a decrease in both anthocyanins and volatile production (Cna'ani et
464 al., 2014; Sood et al., 2021). Indeed, several transcription factors—MYB PH4,
465 PRODUCTION OF ANTHOCYANIN PIGMENT 1 and PhDEF—have been shown to
466 control both pigments and scent (Quattrocchio et al., 2006; Zvi et al., 2008; Zvi et al., 2012;
467 Cna'ani et al., 2015). In this study, we reveal an additional element that regulates these
468 showy traits—the petunia MBW complex. VIGS suppression of the MBW components
469 *AN1* (bHLH) or *AN11* (WDR) in petunia flowers resulted in increased emission of several
470 volatiles from the three branches of phenylalanine-derived volatiles, including a 2-fold rise
471 in methyl benzoate, the main volatile emitted by 'Mitchell' flowers. These results suggest
472 that the MBW complex has a broad negative regulatory role in volatile production. The
473 activity and targets of MBW complexes are dictated by the MYB component (Albert et al.,
474 2011; Albert et al., 2014). Therefore, interactions between volatile-related MYB factors
475 and AN1 and AN11 were tested. Y2H and in-planta pairwise assays revealed that the
476 volatile MYB regulator EOBV interacts directly with AN1. Notably, EOBV, like its
477 *Arabidopsis* homolog AtMYB4 which regulates anthocyanins and interacts with bHLH
478 members, also has the conserved R/B-like bHLH binding motif (Wang et al., 2020). Three-
479 way in-planta protein–protein interaction assays confirmed the formation of the MBW
480 complex consisting of EOBV, AN1 and AN11. MBW components from different plant
481 species have been shown to complement one another (Quattrocchio et al., 1993; de Vetten
482 et al., 1997; Albert et al., 2011). Indeed, ectopic expression of only LacI-AN1 in the
483 pairwise assay, and of LacI-EOBV/AN11-GAL4 and LacI-EOBV/AN1 in the three-way
484 assays, led to weaker activation of the reporter gene in *N. benthamiana* leaves, likely due
485 to the presence of heterologous MBW components.

Spitzer-Rimon et al. (2012) suggested a negative effect of EOBV on floral scent production, although its exact function and mode of action remained unknown. Detailed analyses of volatiles in *eobv*-knockout flowers suggest that EOBV fine-tunes phenylpropene levels: these were significantly increased in the mutant lines relative to control *Cas9* flowers. In contrast, the pools of benzenoids and phenylpropanoid-related compounds was unaltered while their emission decreased, emphasizing the complexity of the machinery responsible for the biosynthesis, intracellular accumulation, transport and release of volatiles (Adebesin et al., 2017; Cna'ani et al., 2017; Liao et al., 2021; Liao et al., 2023; Skaliter et al., 2024). Similar to the *eobv*-suppressed/*eobv*-knockout lines, *AN1*/*AN11* suppression resulted in increased phenylpropene emission. Yet, the emission of C6-C1/C2 volatiles increased in *AN1*/*AN11*-suppressed tissues while their levels were reduced in *eobv*-suppressed tissue. These results indicate that AN1 and AN11 exert a broader influence on volatile production, through direct or indirect mechanisms that are independent of EOBV, potentially by engaging other MYB partners. For example, AN1 and AN11 are necessary for the production of flavonoids, which have been shown to negatively regulate the expression of key phenylpropanoid pathway genes such as *PAL* (Yin et al., 2012). Therefore, suppression of *AN1* or *AN11*, or both, may shift the metabolic balance and alleviate this negative feedback, potentially restoring or enhancing upstream gene expression. Moreover, AN1 has been shown to be involved in the perception/transduction of ethylene signal (Prinsi et al., 2016), and ethylene has been shown to negatively regulate volatiles in petunia (Liu et al., 2017). Notably, the difference in volatile profiles observed following suppression of AN1 or AN11, i.e., the increase in (Z)-isoeugenol detected only in the latter, may be ascribed to the function of WDR proteins as scaffolds anchoring different bHLHs: in petunia, AN11 interacts with JAF13, in addition to AN1 (Albert et al., 2014); in *Arabidopsis*, the WDR TRANSPARENT TESTA GLABRA1 is essential for trichome formation, seed coat pigmentation, and anthocyanin production, with no single bHLH being able to compensate for its loss; in contrast, individual bHLHs such as GLABRA3 or ENHANCER OF GLABRA3 are partially redundant, and their loss typically produces only mild or tissue-specific phenotypes (Ramsay and Glover, 2005).

516 Transcript levels of *C4H2*, encoding the enzyme that controls carbon flux toward
517 phenylpropene biosynthesis, were enhanced in flowers of *eobv* knockouts, in line with
518 phenylpropenes' emission and pool results. Based on our in silico promoter analysis, *ADT3*
519 was also upregulated in *eobv* knockouts, but probably does not have a major impact on
520 total carbon flux as this is not the main *ADT* expressed in mature petunia flowers (Maeda
521 et al., 2010). The promoters of *C4H2* and *ADT3* each contain two repeats of a more specific
522 version of the YACCWACY consensus sequence, which starts with a cytosine and is
523 therefore defined as CACCWACY. Interestingly, several genes carrying only a single copy
524 of CACCWACY (with the exception of *PAL2*): *CS*, *CM*, *PAL1* and *C4H1*, did not show
525 altered expression in the *eobv*-knockout lines. Further experimental analysis will determine
526 whether two CACCWACY elements are required for efficient EOBV-mediated repression
527 of target genes. In contrast to *C4H2* and *ADT3*, which were upregulated in *eobv*-knockout
528 lines, *BSMT* and *PAAS*, which were downregulated, do not contain the YACCWACY motif
529 in their promoters. Because EOBV is a repressor, their downregulation in *eobv* is more
530 likely due to loss of repression of their transcriptional repressors or repression of their
531 activators, or alternatively, due to a feedback loop that prevents toxicity due to
532 hyperaccumulation of volatile organic compounds (Liao et al., 2021; Liao et al., 2023).
533 Despite the facts that *EOBV* and *PhMYB4* have similar diel expression patterns,
534 both regulate *C4H2* and their suppression has a similar effect on volatile emissions, several
535 lines of evidence differentiate them: (1) *ADT3* transcripts were upregulated only in *eobv*-
536 knockout lines; (2) their developmental expression pattern is different (Figs. 5 and 8a); (3)
537 *EOBV* transcripts are enriched in the adaxial epidermis, whereas those of *PhMYB4* are not
538 (Figs. 4d and S10b); (4) knockout of *eobv* had no effect on transcript levels of *PhMYB4*;
539 (5) *PAL* and *C4H1* transcripts were higher in *PhMYB4*-RNAi lines, whereas in the *eobv*
540 knockout, *PAAS* and *BSMT* expression was lower (Colquhoun et al., 2011); (6) EOBV
541 interacted with AN1, but PhMYB4 did not; (7) *PhMYB4* transcripts did not respond to high
542 ambient temperature, in contrast to *EOBV*. Together with analysis of the genomic context
543 (Bombarely et al., 2016), it can be suggested that *EOBV* and *PhMYB4* are paralogs that
544 have probably undergone subfunctionalization. Further experiments are needed to
545 corroborate the exact relations between these two regulators.

546 In addition to spatial, developmental and diel regulation, *EOBV* expression
547 responds to high ambient temperatures. Characterization of *eobv*-knockout lines under
548 long-term exposure to elevated growth temperatures revealed that EOBV is also involved,
549 albeit to a lower extent, in regulating scent production under heat-stress conditions.
550 Transcript levels of EOBV's target, *C4H2*, declined to a similar extent in both *eobv* and
551 *Cas9* flowers under elevated temperatures, regardless of *EOBV*'s increased expression.
552 Furthermore, the observation that *PhMYB4*, which also regulates *C4H2*, remains
553 unaffected by heat suggests that it is also not involved in heat regulation of *C4H2*. Levels
554 of the other EOBV target, ADT3, were slightly, but not significantly reduced in heat-
555 stressed flowers of *Cas9* plants, indicating that it is only mildly affected by elevated
556 temperatures. A similar trend was observed for *ADT3* in *eobv* flowers; however, the
557 reduction was significant, and transcript levels reached those of *Cas9* plants. This likely
558 reflects the higher basal expression of *ADT3* in the knockout lines, rendering it more
559 susceptible to heat-induced downregulation. Cna'ani et al. (2015) showed that in petunia
560 plants grown under elevated temperature, transcript levels of genes encoding enzymes for
561 aromatic amino acid biosynthesis, as well as enzymes dedicated to volatile production,
562 including *C4H*, are drastically reduced, indicating a global plant response aimed at limiting
563 phenylpropanoid biosynthesis. Furthermore, extensive transcriptomic reprogramming that
564 activates the heat-stress response was shown in plants exposed to high temperatures (Chen
565 and Li, 2017). Taken together, these results suggest that EOBV does not mediate the heat
566 regulation of *C4H2* or *ADT3*, and that both are regulated as part of a broader temperature-
567 responsive network.
568 Heat is a key environmental factor that has been shown to negatively impact flower
569 size in various plants (Descamps et al., 2018; Sood et al., 2021; Wiszniewski et al., 2022).
570 In this study, we show that EOBV is involved in determining final flower size under heat-
571 stress conditions; the reduction in corolla size caused by high temperatures was mitigated
572 in *eobv*-knockout compared to control *Cas9* plants. Although *EOBV* transcripts are
573 enriched in the adaxial epidermis under standard growth conditions, there was no
574 differential effect on the development of adaxial versus abaxial sides, as overall floral
575 morphology remained normal at high temperature. It would be informative to test *EOBV*
576 bilateral expression in the petal epidermis at different stages of flower development,

577 especially under high-temperature conditions, as well as its post-
578 transcriptional/translational regulation. It is worth noting that *cycloidea* mutants in
579 *Antirrhinum majus* (Snapdragon) have smaller petals although, like EOBV, *CYCLOIDEA*
580 is expressed predominantly in the adaxial epidermis (Luo et al., 1996).

581 Flower cells undergo proliferation and expansion during the early and late stages
582 of bud development, respectively, both of which have been shown to be impacted by
583 elevated temperatures (Sood et al., 2021). Indeed, expression of petunia *PhEXP1*, which
584 plays a key role in cell expansion, was reduced in flowers exposed to high temperature
585 (Fig.13) (Zenoni et al., 2004). However, its expression was similarly reduced in both *eobv*
586 and *Cas9* flowers at 28°C, suggesting that the limited reduction in petal size observed in
587 *eobv* under elevated temperatures was not due to misregulation of *PhEXP1*, and that the
588 effect on flower size may be mediated by additional factors downstream or independent of
589 PhEXP1. Sood et al. (2021) demonstrated that in petunia, increased levels of abscisic acid
590 affect early stages of bud development in response to elevated temperatures and likely
591 antagonize cytokinin-promoted cell division. Interestingly, crosstalk between abscisic acid
592 and the MBW complex has been demonstrated in several plants (Lama et al., 2020;
593 Broucke et al., 2023). Moreover, our in silico promoter analysis revealed that the promoters
594 of several genes linked to hormones contain repeats of the YACCWACY motif, found in
595 targets of EOBV. Two repeats of this motif were also found in a homolog of the
596 *Arabidopsis* MADS-box transcription factor *SHORT VEGETATIVE PHASE*, a heat-
597 sensitive repressor of *FLOWERING LOCUS T*; mutations in the latter have been shown to
598 result in smaller petals (Jeong et al., 2007; Romera-Branchat et al., 2025). Thus, at early
599 stages, EOBV might modulate the expression of genes related to flower
600 initiation/development, and this modulation could become dysregulated under heat stress,
601 leading to changes in petal size. The interaction of EOBV with the components of the
602 MBW complex, involved in the control of floral showy traits, further interlinks flower
603 development with the environment.
604

605 **Materials and methods**

606

607 **Plant material and growth conditions**

608

609 *Petunia* × *hybrida* cv. Mitchell diploid plants were grown from seeds. Rooted plants of
610 *Petunia* × *hybrida* cv. Classic Blue Ray were obtained from Danziger – "Dan" Flower
611 Farm (Mishmar Hashiva, Israel). Plants were grown in a greenhouse under 25°C
612 day/20°C night temperatures with a 16 h light/8 h dark photoperiod [incandescent light
613 bulbs (120 V, 16 lm/W) were used to provide additional lighting].
614 For the elevated growth temperature experiment, *eobv*-knockout line #1 and
615 control *Cas9* seedlings were sown and grown for a month under standard conditions
616 (25/20°C day/night). Then, plants from each treatment, which had not yet developed
617 floral buds, were separated into two groups and transferred to a phytotron greenhouse
618 (16/8 h light/dark photoperiod) with controlled rooms: one group from each treatment at
619 22/16°C day/night and the other at 28/22°C. After a month, 2DPA flowers were taken for
620 diameter measurement with a Vernier caliper (Mitutoyo, Kanagawa, Japan), and
621 headspace, internal pool and RT-qPCR analyses.
622 *N. benthamiana* plants were kindly provided by Dr. Guy Polturak (Institute of
623 Plant Sciences and Genetics in Agriculture, The Robert H. Smith Faculty of Agriculture,
624 Food and Environment, The Hebrew University of Jerusalem) and maintained in a
625 controlled growth room at 22°C under a 16 h light/8 h dark photoperiod with fluorescent
626 lighting.
627

628 **RNA extraction and RT-qPCR analyses**

629

630 Total RNA was extracted from 30–100 mg of ground (with liquid nitrogen) floral tissues
631 using the Tri-Reagent kit (Sigma-Aldrich) and treated with RNase-free DNase I (Thermo
632 Fisher Scientific). First-strand cDNA was synthesized using total RNA, oligo(dT) primer,
633 and reverse transcriptase ImProm-II (Promega, Madison, WI, USA) according to the
634 manufacturer's instructions. Two-step real-time qPCR was performed on a CFX Opus 384
635 Real-Time PCR System (Bio-Rad, Hercules, CA, USA) using 2X qPCRBIO SyGreen Blue
636 Mix Hi-ROX (PCR Biosystems, London, UK). A standard curve was generated for each
637 gene using dilutions of cDNA samples, and data analysis was performed using Bio-Rad
638 CFX Maestro software (Bio-Rad, Hercules, CA, USA). Primer specificity was determined

639 by melting-curve analysis. Raw transcript-level data were normalized to the geomean of
640 *EF1α*, *UBIQUITIN* and *ACTIN*. Quantification calculations were carried out using the
641 $2^{-\Delta\Delta CT}$ formula. Primers are shown in Table S2.
642
643 **VIGS suppression of target genes in petunia flowers**
644
645 A 162-bp fragment of the 3' UTR of *EOBV*, a 332-bp fragment of AN11's 3' UTR and a
646 250-bp fragment of AN1's 3' UTR were amplified and cloned into pTRV2.
647 *Agrobacterium tumefaciens* strain AGL0 was transformed with plasmids harboring
648 RNA1 (pTRV1), pTRV2-EOBV, pTRV2-AN1, pTRV2-AN11 or pTRV2-CHS as a
649 control. *Agrobacterium* carrying pTRV1 were mixed at a 1:1 ratio (to OD_{600} = 0.5) with
650 *Agrobacterium* carrying the above-mentioned plasmids in inoculation solution containing
651 200 µm acetosyringone and 10 mm $MgCl_2$. Corollas of petunia cv. Mitchell flowers at
652 anthesis were inoculated with the *Agrobacterium* solutions by piercing with a needle and
653 infiltration using a syringe, followed by localized headspace analysis as described in
654 Skaliter et al. (2021).
655 To determine EOBV's effect on anthocyanin content in petunia cv. P720, cultures
656 of *Agrobacterium* transformed with pTRV1 and pTRV2-EOBV or pTRV2-CHS were
657 grown overnight at 28°C in LB Broth Lennox medium (Formedium, Norfolk, UK)
658 supplemented with 50 mg/L kanamycin and 200 µM acetosyringone. The cells were
659 harvested and resuspended in inoculation buffer containing 10 mM MES, pH 5.5, 200 µM
660 acetosyringone, and 10 mM $MgCl_2$ to an OD_{600} of 10. Following an additional 3 h of
661 incubation at 28°C, the bacteria containing pTRV1 were mixed with those containing the
662 pTRV2 derivatives in a 1:1 ratio; 400 µL of this mixture was applied to the cut surface,
663 after removing the apical meristem, of 1-month-old petunia 'P720' plants.
664
665 **Collection of emitted volatiles, internal pools and GC–MS analysis**
666
667 Dynamic headspace analysis was performed by harvesting flowers 2DPA and placing
668 them in a 50-mL beaker filled with tap water in jars (2 flowers per jar). Volatiles were
669 collected for 24 h using columns made of glass tubes containing 100 mg Porapak Q

670 polymer and 100 mg 20/40-mesh, held in place with plugs of silanized glass wool.
671 Trapped volatiles were eluted with 1.5 mL hexane and 0.5 mL acetone. Isobutylbenzene
672 was used as an internal standard.
673 To determine the pool sizes of volatile compounds, 100 mg tissue from 1DPA
674 flowers was ground in liquid nitrogen and extracted in 400 μL hexane containing
675 isobutylbenzene as the internal standard. Following 2 h of incubation with gentle shaking
676 at 25 °C, extracts were centrifuged at 10,500× g for 10 min, and the supernatant was
677 further centrifuged, followed by GC–MS analysis.
678 GC–MS analysis (of a 1 μL sample) was performed using a device consisting of a
679 PAL autosampler (CTC Analytics, Zwingen, Switzerland), a TRACE GC 2000 gas
680 chromatograph (Thermo Fisher Scientific, Waltham, MA, USA) equipped with an Rtx-
681 5SIL mass spectrometer fused-silica capillary column (inner diameter 0.25 μm, 30 m ×
682 0.25 mm; Restek, Centre County, PA, USA), and a TRACE DSQ quadruple mass
683 spectrometer (Thermo Fisher Scientific, Waltham, MA, USA). Helium was used as the
684 carrier gas at a flow rate of 1 mL/min. The injector temperature was set to 220 °C
685 (splitless mode), the interface to 240 °C, and the ion source to 200 °C. The analysis was
686 performed under the following temperature program: 2 min of isothermal heating at 40
687 °C followed by a 7 °C/min oven temperature ramp to 250 °C, then 2 min of isothermal
688 heating. The system was equilibrated for 1 min at 70 °C before injecting the next sample.
689 Mass spectra were recorded at 3.15 scans/s with a scanning range of 40–350 mass-to-
690 charge ratio and electron energy of 70 eV. Compounds were tentatively identified (>95%
691 match) based on NIST/EPA/NIH Mass Spectral Library data version NIST 17 (with
692 software version 3.4) using xcalibur 1.3 (Thermo Fisher Scientific, Waltham, MA, USA).
693 Further identification of all compounds was based on a comparison of mass spectra and
694 retention times with those of authentic standards (Sigma-Aldrich, St. Louis, MO, USA)
695 analyzed under similar conditions.
696
697 **Protein–protein interaction assays**
698
699 **Y2H assay**

700 The coding sequences of the tested genes were cloned to either the GAL4 BD in the
701 pBD-GAL4 CAM vector (Clontech) or the GAL4 AD in pACT2 (Takara Bio, Mountain
702 View, CA,USA) and transformed into *Saccharomyces cerevisiae* strain Y190.
703 Transformed yeast were grown on synthetic defined medium (SD) lacking leucine and/or
704 tryptophan for selection. Interaction between targets was detected by dripping 2.5-μL
705 drops of individual clones on SD media lacking leucine and tryptophan followed by
706 incubation at 28°C for 48 h. Formed colonies were gently covered with chloroform and
707 incubated for 15 min at room temperature, and then the chloroform was drained. Colonies
708 were gently covered with staining solution (containing X-Gal) and monitored for β-
709 galactosidase reporter gene expression levels after 1 h.
710
711 **In-planta protein-interaction assays**
712
713 All vectors were constructed using GoldenBraid 2.0 (Sarrion-Perdigones et al., 2013). The
714 *RUBY* open-reading frame (He et al., 2020) was cloned under the 6×LacI operon fused to
715 the CaMV 35S minimal promoter (pDGB3α1-pOpLacI:mini35S:*RUBY*). *AN1* was fused
716 with the LacI BD into pDGB3α1 or cloned into pDGB3 3Ω1 containing *DsRed*, and *AN11*
717 was fused with the GAL4 AD. EOBV was fused with either GAL4 AD or LacI BD into
718 pDGB3α2. *Agrobacterium* were mixed (to OD_{600} = 0.5) and third or fourth leaves of *N.*
719 *benthamiana* plants or *N. tabacum* disc explants were inoculated and placed on
720 regeneration media. In the three-way protein–protein interaction assays, inoculated *N.*
721 *benthamiana* leaves were examined under a fluorescent stereomicroscope (SMZ1270;
722 Nikon, Minato City, Tokyo, Japan) for DsRed detection. Inoculated leaves of both pairwise
723 and three-way assays were harvested 5 days postinoculation, and 3 disks of each leaf (0.8
724 cm diameter) were taken for analysis and immersed in 100% ethanol until the tissue was
725 completely bleached. Betalains were extracted from the tissue by the addition of 1 mL
726 DDW and placed on an orbital shaker (150 rpm) at room temperature for 3 h. The light
727 absorbance of the extract was measured in a Multiskan SkyHigh Microplate
728 Spectrophotometer (Thermo Fisher Scientific, Waltham, MA, USA) at 538 nm. For *N.*
729 *tabacum*, 2 weeks postinoculation, calli formed from inoculated explants were bleached in

730 100% ethanol for 2 days and observed under a stereomicroscope (SMZ1270; Nikon,
731 Minato City, Tokyo, Japan).

732 **Phylogenetic analysis**

733

734 Protein sequences were aligned using the Clustal W algorithm (Larkin et al., 2007)
735 implemented in MEGA11 (Tamura et al., 2021) with default parameters (gap opening
736 penalty 10.00; gap extension penalty 0.20). Maximum likelihood with default parameters
737 (1000 bootstraps; Jones–Taylor–Thornton substitution model) was used as the statistical
738 method for phylogenetic analysis in MEGA11.

739

740 **EOBV localization assay**

741

742 The coding sequence of *EOBV* (without the stop codon) was amplified from cDNA
743 extracted from flowers and fused to GFP using a GoldenBraid 2.0 reaction (Sarrion-
744 Perdigones et al., 2013) to generate pDGB3α2-EOBV-GFP and pDGB3α2-GFP-EOBV.
745 'Mitchell' flowers at anthesis were inoculated with a mixture of *Agrobacterium* carrying
746 pDGB3α2-EOBV-GFP and pRCS-RFP-VirD2-NLS (marker for nuclear localization) or
747 pDGB3α2-GFP-EOBV and pRCS-RFP-VirD2-NLS, or pDGB3α2-EOBV-GFP alone and
748 pRCS-RFP-VirD2-NLS alone as a control. Inoculated flowers were harvested 2DPA.
749 Images were acquired with a Leica SP8 laser scanning microscope equipped with solid-
750 state lasers with 488 nm (GFP excitation) and 552 nm (RFP excitation) light, an HC PL
751 APO CS 63x/1.2 water-immersion objective and Leica Application Suite X software
752 (LASX) (Leica Microsystems, Wetzlar, Germany). GFP- and RFP-emission signals were
753 detected with HyD (hybrid) detectors in the ranges of 500–540 and 565–640 nm,
754 respectively. Merged images were generated using Fiji (Image J) software (Rueden et al.,
755 2017).

756

757 **Anthocyanin content**

758

759 To determine anthocyanin levels, 100 mg of corollas of petunia cv. Classic Blue Ray
760 inoculated with TRV2-EOBV or TRV2-CHS were ground (with liquid nitrogen),

761 incubated with acidic methanol (containing 1% v/v HCl) and placed on an orbital shaker
762 (150 rpm) at 4°C for 2 h in the dark. The light absorbance of the extracts was measured in
763 a spectrophotometer (Multiskan SkyHigh spectrophotometer; Thermo Fisher Scientific,
764 Waltham, MA, USA) at 530 nm (anthocyanins) and 657 nm (chlorophyll). Anthocyanin
765 content was calculated using the using the formula $A_{530} – 0.25(A_{657})$.
766
767 **Generation of *eobv*-knockout lines**
768
769 Tobacco rattle virus RNA2 (pTRV2) vectors pTRV2-sgRNA1-sgRNA2 and pTRV2-
770 sgRNA1-sgRNA3, were synthesized by Twist Bioscience (San Francisco, CA, USA),
771 based on the pTRV2 vector with GenBank accession AF406991. Nuclease-potent *Cas9*
772 line #2 (harboring AtUbqp(1460): human-optimized Cas9/Nosp:NPTII) was used as the
773 platform for generating *eobv*-knockout lines, as described in Skaliter et al. (2024). Sterile
774 explants of *Cas9* line #2 were inoculated with *A. tumefaciens* strain AGL0 harboring
775 pTRV2-*sgRNA1*-s*gRNA2* or pTRV2-*sgRNA1-sgRNA3* and pTRV1 (AF406990). Explants
776 were incubated for 20 min in the *Agrobacterium* suspension (in Luria-Bertani broth)
777 containing 100 µm acetosyringone, followed by incubation in the dark for 3 days on
778 Murashige and Skoog (MS) medium supplemented with 3% (w/v) sucrose, followed by
779 transfer for selection on MS with 3% sucrose, antibiotics (kanamycin, carbenicillin) and
780 phytohormones (1.5 mg/L benzylaminopurine [BA], 0.15 mg/L naphthalene acetic acid
781 [NAA]), and incubated under a 12 h light/12 h dark photoperiod at 22°C until
782 regeneration and elongation of regenerants. The medium was renewed every 2 weeks. At
783 the elongation stage, the BA concentration was decreased to 1 mg/L. To switch
784 regenerants to rooting, they were transferred to medium without BA, supplemented with
785 0.25 mg/L NAA. To screen the gene-edited plantlets, genomic DNA was extracted from
786 them using the CTAB method followed by PCR and Sanger sequencing. Positive plants
787 (T0) were grown on MS with 3% sucrose, transferred to the greenhouse and self-
788 pollinated. Progeny (T1) plants were molecularly analyzed and self-pollinated. The T2
789 population was screened for homozygous plants, which were selected for further
790 analyses.
791

792 **In silico promoter analysis**

793

794 Extraction of promoter regions of the *P. axillaris* genome (https://solgenomics.net/) and
795 motif analysis were performed using Python (https://www.python.org/). The code was
796 developed with assistance from ChatGPT and is available at:
797 https://github.com/OdedSkaliter/Promoter-extraction-and-motif-analysis-Petunia-
798 genome.

799

800 **Statistical analysis**

801

802 Statistical analyses were performed using JMP Pro 18 (SAS, Cary, NC, USA).

803

804 **Data availability**

805 The data underlying this article will be shared on reasonable request to the corresponding
806 author.

807

808 **Funding**

809 This work was supported by the Israel Science Foundation (grant no. 1368/23). A.V. is an
810 incumbent of the Wolfson Chair in Floriculture.

811

812 **Author contributions**

813 O.S. conceptualized, planned and designed the research, performed experiments, analyzed
814 data, and wrote the manuscript. Ek.S., E.L.L., O.R., R.C., El.S., E.M., T.M. and O.E.
815 performed experiments and analyzed data. A.V. conceptualized, planned and designed the
816 research and wrote the manuscript. All authors revised the manuscript and approved the
817 final version.

818

819 **Acknowledgments**

820 We thank Danziger – "Dan" Flower Farm for providing petunia cv. Blue Ray plants. We
821 also thank Dr. Guy Polturak (Institute of Plant Sciences and Genetics in Agriculture, The
822 Robert H. Smith Faculty of Agriculture, Food and Environment, The Hebrew University

of Jerusalem) for providing *N. benthamiana* plantlets and his assistance with the betalain extraction. During the preparation of this manuscript, the authors used ChatGPT (OpenAI, GPT-5.1, 2026) to assist with language editing and text refinement. All AI-assisted content was reviewed and revised by the authors, who take full responsibility for the final version of the manuscript.

Competing interests

The authors declare no competing interests.

Supplemental material

Figure S1. Virus-induced gene silencing (VIGS) of *AN1* and *AN11* in petunia.

Figure S2. Yeast-two hybrid assay testing the interactions of various MYB regulators of volatile production with AN1 and AN11.

Figure S3. Protein domain analysis of EOBV.

Figure S4. EOBV participates in the MBW complex.

Figure S5. EOBV is an R2R3-MYB subgroup 4 member.

Figure S6. *EOBV* expression levels in petunia floral buds and flowers 1 day postanthesis (1DPA) in the morning (1000 h) and evening (1900 h).

Figure S7. Virus-induced gene silencing (VIGS) of *EOBV* in petunia flowers.

Figure S8. Effect of exogenous gibberellin (GA) application on *EOBV* transcripts.

Figure S9. In silico promoter analysis in the *Petunia axillaris* genome.

854 Figure S10. Diel, developmental and spatial expression patterns of PhMYB4.

855

856 Figure S11. *PhMYB4* genomic sequence is not affected by knockout of *eobv*.

857

858 Figure S12. Stacking of *ever*- and *eobv*-knockout alleles.

859

860 Figure S13. Effect of elevated growth temperature regime on expression of *PhMYB4* and
861 α-expansin (*PhEXP1*) in *eobv*-knockout lines.

862

863 Supplementary Table 1. Promoters of genes in the *Petunia axillaris* genome containing the
864 motif YACCWACY.

865

866 Supplementary Table 2. List of primers used in this study.

867

868 **References**

869 **Adebesin F, Widhalm JR, Boachon B, Lefèvre F, Pierman B, Lynch JH, Alam I,**
870 **Junqueira B, Benke R, Ray S, et al** (2017) Emission of volatile organic
871 compounds from petunia flowers is facilitated by an ABC transporter. Science **356**:
872 1386–1388.

873 **Agarwal P, Mitra M, Banerjee S, Roy S** (2020) MYB4 transcription factor, a member
874 of R2R3-subfamily of MYB domain protein, regulates cadmium tolerance via
875 enhanced protection against oxidative damage and increases expression of PCS1 and
876 MT1C in Arabidopsis. Plant Sci **297**: 110501.

877 **Albert NW, Davies KM, Lewis DH, Zhang H, Montefiori M, Brendolise C, Boase**
878 **MR, Ngo H, Jameson PE, Schwinn KE** (2014) A conserved network of
879 transcriptional activators and repressors regulates anthocyanin pigmentation in
880 Eudicots. Plant Cell **26**: 962–980.

881 **Albert NW, Lewis DH, Zhang H, Schwinn KE, Jameson PE, Davies KM** (2011)
882 Members of an R2R3-MYB transcription factor family in Petunia are
883 developmentally and environmentally regulated to control complex floral and
884 vegetative pigmentation patterning. Plant J **65**: 771–784.

885 **Bednarczyk D, Skaliter O, Kerzner S, Masci T, Shklarman E, Shor E, Vainstein A**
886 (2025) The homeotic gene *PhDEF* regulates production of volatiles in petunia
887 flowers by activating *EOBI* and *EOBII*. Plant Cell **37**: 1–12.

888 **Ben-Nissan G, Lee JY, Borohov A, Weiss D** (2004) GIP, a Petunia hybrida GA-induced
889 cysteine-rich protein: A possible role in shoot elongation and transition to flowering.

890 Plant J **37**: 229–238.

891 **Blum M, Chang HY, Chuguransky S, Grego T, Kandasaamy S, Mitchell A, Nuka G,**
892 **Paysan-Lafosse T, Qureshi M, Raj S, et al** (2021) The InterPro protein families
893 and domains database: 20 years on. Nucleic Acids Res **49**: D344–D354.

894 **Bombarely A, Moser M, Amrad A, Bao M, Bapaume L, Barry CS, Bliek M,**
895 **Boersma MR, Borghi L, Bruggmann R, et al** (2016) Insight into the evolution of
896 the Solanaceae from the parental genomes of *Petunia hybrida*. Nat Plants **2**: 1–9.

897 **Broucke E, Dang TTV, Li Y, Hulsmans S, Van Leene J, De Jaeger G, Hwang I,**
898 **Wim V den E, Rolland F** (2023) SnRK1 inhibits anthocyanin biosynthesis through
899 both transcriptional regulation and direct phosphorylation and dissociation of the
900 MYB/bHLH/TTG1 MBW complex. Plant J **115**: 1193–1213.

901 **Bulanov AN, Andreeva EA, Tsvetkova N V., Zykin PA** (2025) Regulation of flavonoid
902 biosynthesis by the MYB-bHLH-WDR (MBW) complex in plants and its specific
903 features in cereals. Int J Mol Sci. **26**: 734.

904 **Chen J, Luo M, Hands P, Rolland V, Zhang J, Li Z, Outram M, Dodds P, Ayliffe M**
905 (2023) A split GAL4 RUBY assay for visual in planta detection of protein–protein
906 interactions. Plant J **114**: 1209–1226.

907 **Chen L, Hu B, Qin Y, Hu G, Zhao J** (2019) Advance of the negative regulation of
908 anthocyanin biosynthesis by MYB transcription factors. Plant Physiol Biochem **136**:
909 178–187.

910 **Chen S, Li H** (2017) Heat stress regulates the expression of genes at transcriptional and
911 post-transcriptional levels, revealed by RNA-seq in *Brachypodium distachyon*. Front
912 Plant Sci **7**: 1–13.

913 **Cna'ani A, Mühlemann JK, Ravid J, Masci T, Klempien A, Nguyen TTH, Dudareva**
914 **N, Pichersky E, Vainstein A** (2014) *Petunia × hybrida* floral scent production is
915 negatively affected by high-temperature growth conditions. Plant, Cell Environ **38**:
916 1333–1346.

917 **Cna'ani A, Shavit R, Ravid J, Aravena-Calvo J, Skaliter O, Masci T, Vainstein A**
918 (2017) Phenylpropanoid scent compounds in *Petunia x hybrida* are glycosylated and
919 accumulate in vacuoles. Front Plant Sci **8**: 1–14.

920 **Cna'ani A, Spitzer-Rimon B, Ravid J, Farhi M, Masci T, Aravena-Calvo J, Ovadis**
921 **M, Vainstein A** (2015) Two showy traits, scent emission and pigmentation, are
922 finely coregulated by the MYB transcription factor PH4 in petunia flowers. New
923 Phytol **208**: 708–714.

924 **Colquhoun TA, Kim JY, Wedde AE, Levin LA, Schmitt KC, Schuurink RC, Clark**
925 **DG** (2011) PhMYB4 fine-tunes the floral volatile signature of *Petunia×hybrida*
926 through PhC4H. J Exp Bot **62**: 1133–1143.

927 **Concordet JP, Haeussler M** (2018) CRISPOR: Intuitive guide selection for
928 CRISPR/Cas9 genome editing experiments and screens. Nucleic Acids Res **46**:
929 W242–W245.

930 **Descamps C, Quinet M, Baijot A, Jacquemart AL** (2018) Temperature and water
931 stress affect plant–pollinator interactions in *Borago officinalis* (Boraginaceae). Ecol
932 Evol **8**: 3443–3456.

933 **Dubos C, Stracke R, Grotewold E, Weisshaar B, Martin C, Lepiniec L** (2010) MYB
934 transcription factors in Arabidopsis. Trends Plant Sci **15**: 573–581.

935 **Espley R V., Brendolise C, Chagné D, Kutty-Amma S, Green S, Volz R, Putterill J,**
936 **Schouten HJ, Gardiner SE, Hellens RP, et al** (2009) Multiple repeats of a
937 promoter segment causes transcription factor autoregulation in red apples. Plant Cell
938 **21**: 168–183.

939 **Gübitz, T. Hoballah, M.E. Dell'Olivo, A. Kuhlemeier C** (2009) in Petunia:
940 Evolutionary, Developmental and Physiological Genetics (eds. Gerats, T. &
941 Strommer, J.). Petunia Evol Dev Physiol Genet (eds Gerats, T Strommer, J). doi:
942 10.1007/978-0-387-84796-2.

943 **He Y, Zhang T, Sun H, Zhan H, Zhao Y** (2020) A reporter for noninvasively
944 monitoring gene expression and plant transformation. Hortic Res **7**: 1–6.

945 **Jeong HL, Seong JY, Soo HP, Hwang I, Jong SL, Ji HA** (2007) Role of SVP in the
946 control of flowering time by ambient temperature in Arabidopsis. Genes Dev **21**:
947 397–402.

948 **Jin H, Cominelli E, Bailey P, Parr A, Mehrtens F, Jones J, Tonelli C, Weisshaar B,**
949 **Martin C** (2000) Transcriptional repression by AtMYB4 controls production of
950 UV-protecting sunscreens in Arabidopsis. EMBO J **19**: 6150.

951 **Lama K, Harlev G, Shafran H, Peer R, Flaishman MA** (2020) Anthocyanin
952 accumulation is initiated by abscisic acid to enhance fruit color during fig (F*icus*
953 *carica* L.) ripening. J Plant Physiol **251**: 153192.

954 **Larkin MA, Blackshields G, Brown NP, Chenna R, Mcgettigan PA, McWilliam H,**
955 **Valentin F, Wallace IM, Wilm A, Lopez R, et al** (2007) Clustal W and Clustal X
956 version 2.0. Bioinformatics **23**: 2947–2948.

957 **Liao P, Maoz I, Shih M-LL, Lee JH, Huang X-QQ, Morgan JA, Dudareva N** (2023)
958 Emission of floral volatiles is facilitated by cell-wall non-specific lipid transfer
959 proteins. Nat Commun **14**: 330.

960 **Liao P, Ray S, Boachon B, Lynch JH, Deshpande A, McAdam S, Morgan JA,**
961 **Dudareva N** (2021) Cuticle thickness affects dynamics of volatile emission from
962 petunia flowers. Nat Chem Biol **17**: 138–145.

963 **Liu F, Xiao Z, Yang L, Chen Q, Shao L, Liu J, Yu Y** (2017) PhERF6, interacting with
964 EOBI, negatively regulates fragrance biosynthesis in petunia flowers. New Phytol
965 **215**: 1490–1502.

966 **Luha R, Rana V, Vainstein A, Kumar V** (2024) Nonsense-mediated mRNA decay
967 pathway in plants under stress: general gene regulatory mechanism and advances.
968 Planta **259**: 1–18.

969 **Luo D, Carpenter R, Vincent C, Copsey L, Coen E** (1996) Origin of floral asymmetry
970 in *Antirrhinum*. Nature **383**: 794–799.

971 **Lynch JH, Qian Y, Guo L, Maoz I, Huang XQ, Garcia AS, Louie G, Bowman ME,**
972 **Noel JP, Morgan JA, et al** (2020) Modulation of auxin formation by the cytosolic
973 phenylalanine biosynthetic pathway. Nat Chem Biol **16**: 850–856.

974 **Ma D, Constabel CP** (2019) MYB repressors as regulators of phenylpropanoid
975 metabolism in plants. Trends Plant Sci **24**: 275–289.

976 **Maeda H, Shasany AK, Schnepp J, Orlova I, Taguchi G, Cooper BR, Rhodes D,**
977 **Pichersky E, Dudareva N** (2010) RNAi suppression of *arogenate dehydratase1*
978 reveals that phenylalanine is synthesized predominantly via the arogenate pathway
979 in Petunia petals. Plant Cell **22**: 832–849.

980 **Muhlemann JK, Klempien A, Dudareva N** (2014) Floral volatiles: From biosynthesis
981 to function. Plant, Cell Environ **37**: 1936–1949.

982 **Ohta M, Matsui K, Hiratsu K, Shinshi H, Ohme-Takagi M** (2001) Repression
983 domains of class II ERF transcriptional repressors share an essential motif for Active
984 repression. Plant Cell **13**: 1959.

985 **Patrick RM, Huang X-Q, Dudareva N, Li Y** (2021) Dynamic histone acetylation in
986 floral volatile synthesis and emission in petunia flowers. J Exp Bot **72**: 3704–3722.

987 **Prinsi B, Negri AS, Quattrocchio FM, Koes RE, Espen L** (2016) Proteomics of red
988 and white corolla limbs in petunia reveals a novel function of the anthocyanin
989 regulator ANTHOCYANIN1 in determining flower longevity. J Proteomics **131**:
990 38–47.

991 **Quattrocchio F, Verweij W, Kroon A, Spelt C, Mol J, Koes R** (2006) PH4 of petunia
992 is an R2R3 MYB protein that activates vacuolar acidification through interactions
993 with basic-helix-loop-helix transcription factors of the anthocyanin pathway. Plant
994 Cell **18**: 1274–1291.

995 **Quattrocchio F, Wing J, van der Woude K, Souer E, de Vetten N, Mol J, Koes R**
996 (1999) Molecular analysis of the *anthocyanin2* gene of petunia and its role in the
997 evolution of flower color. Plant Cell **11**: 1433–1444.

998 **Quattrocchio F, Wing JF, Leppen HTC, Mol JNM, Koes RE** (1993) Regulatory genes
999 controlling anthocyanin pigmentation are functionally conserved among plant
1000 species and have distinct sets of target genes. Plant Cell **5**: 1497–1512.

1001 **Ramsay NA, Glover BJ** (2005) MYB-bHLH-WD40 protein complex and the evolution
1002 of cellular diversity. Trends Plant Sci **10**: 63–70.

1003 **Ravid J, Spitzer-Rimon B, Takebayashi Y, Seo M, Cna'ani A, Aravena-Calvo J,**
1004 **Masci T, Farhi M, Vainstein A** (2017) GA as a regulatory link between the showy
1005 floral traits color and scent. New Phytol **215**: 411–422.

1006 **Romera-Branchat M, Pocard C, Vincent C, Cerise M, da Silveira Falavigna V,**
1007 **Pajoro A, Ding N, Gao H, Franzen R, Coupland G** (2025) FD and FDP bZIP

1008 transcription factors and FT florigen regulate floral development and control
1009 homeotic gene expression in Arabidopsis floral meristems. Development. **32**:
1010 107966.

1011 **Rueden CT, Schindelin J, Hiner MC, DeZonia BE, Walter AE, Arena ET, Eliceiri**
1012 **KW** (2017) ImageJ2: ImageJ for the next generation of scientific image data. BMC
1013 Bioinformatics **18**: 1–26.

1014 **Sarrion-Perdigones A, Vazquez-Vilar M, Palací J, Castelijns B, Forment J, Ziarsolo**
1015 **P, Blanca J, Granell A, Orzaez D** (2013) Goldenbraid 2.0: A comprehensive DNA
1016 assembly framework for plant synthetic biology. Plant Physiol **162**: 1618–1631.

1017 **Shaipulah NFM, Muhlemann JK, Woodworth BD, Van Moerkercke A, Verdonk**
1018 **JC, Ramirez AA, Haring MA, Dudareva N, Schuurink RC** (2016) *CCoAOMT*
1019 down-regulation activates anthocyanin biosynthesis in petunia. Plant Physiol **170**:
1020 717–731.

1021 **Shor E, Ravid J, Sharon E, Skaliter O, Masci T, Vainstein A** (2023a) SCARECROW-
1022 like GRAS protein PES positively regulates petunia floral scent production. Plant
1023 Physiol **192**: 409–425.

1024 **Shor E, Skaliter O, Sharon E, Kitsberg Y, Bednarczyk D, Kerzner S, Vainstein D,**
1025 **Tabach Y, Vainstein A** (2023b) Developmental and temporal changes in petunia
1026 petal transcriptome reveal scent-repressing plant-specific RING–kinase–WD40
1027 protein. Front Plant Sci **14**: 1180899.

1028 **Shor E, Vainstein A** (2024) Petunia PHYTOCHROME INTERACTING FACTOR 4/5
1029 transcriptionally activates key regulators of floral scent. Plant Mol Biol. doi:
1030 10.1007/s11103-024-01455-8.

1031 **Skaliter O, Bednarczyk D, Shor E, Shklarman E, Manasherova E, Aravena-Calvo J,**
1032 **Kerzner S, Cna'ani A, Jasinska W, Masci T, et al** (2024) The R2R3-MYB
1033 transcription factor EVER controls the emission of petunia floral volatiles by
1034 regulating epicuticular wax biosynthesis in the petal epidermis. Plant Cell **36**: 174–
1035 193.

1036 **Skaliter O, Gura A, Livneh Y, Cohen R, Shklarman E, Edelbaum O, Masci T,**
1037 **Vainstein A** (2026) Targeted Gene modification of *HMGR* enhances biosynthesis of
1038 terpenoid and phenylpropanoid volatiles in petunia and lettuce. Int J Mol Sci **27**:
1039 1522.

1040 **Skaliter O, Kitsberg Y, Sharon E, Shklarman E, Shor E, Masci T, Yue Y, Arien Y,**
1041 **Tabach Y, Shafir S, et al** (2021) Spatial patterning of scent in petunia corolla is
1042 discriminated by bees and involves the ABCG1 transporter. Plant J **106**: 1746–1758.

1043 **Skaliter O, Livneh Y, Agron S, Shafir S, Vainstein A** (2022) A whiff of the future:
1044 Functions of phenylalanine-derived aroma compounds and advances in their
1045 industrial production. Plant Biotechnol J **20**: 1651–1669

1046 **Sood A, Duchin S, Adamov Z, Carmeli-Weissberg M, Shaya F, Spitzer-Rimon B**
1047 (2021) Abscisic acid mediates the reduction of petunia flower size at elevated

1048 temperatures due to reduced cell division. Planta **255**: 1–14.

1049 **Spelt C, Quattrocchio F, Mol JNM, Koes R** (2000) *Anthocyanin1* of petunia encodes a
1050 basic helix-loop-helix protein that directly activates transcription of structural
1051 anthocyanin genes. Plant Cell **12**: 1619–1631.

1052 **Spitzer-Rimon B, Farhi M, Albo B, Cna'ani A, Ben Zvi MM, Masci T, Edelbaum O,**
1053 **Yu Y, Shklarman E, Ovadis M, et al** (2012) The R2R3-MYB-like regulatory
1054 factor EOBI, acting downstream of EOBII, regulates scent production by activating
1055 *ODO1* and structural scent-related genes in petunia. Plant Cell **24**: 5089–5105.

1056 **Spitzer-Rimon B, Marhevka E, Barkai O, Marton I, Edelbaum O, Masci T,**
1057 **Prathapani NK, Shklarman E, Ovadis M, Vainstein A** (2010) *EOBII*, a gene
1058 encoding a flower-specific regulator of phenylpropanoid volatiles' biosynthesis in
1059 petunia. Plant Cell **22**: 1961–1976.

1060 **Spitzer B, Zvi MM Ben, Ovadis M, Marhevka E, Barkai O, Edelbaum O, Marton I,**
1061 **Masci T, Alon M, Morin S, et al** (2007) Reverse genetics of floral scent:
1062 Application of tobacco rattle virus-based gene silencing in petunia. Plant Physiol
1063 **145**: 1241–1250.

1064 **Sturme MHJ, Van Der Berg JP, Bouwman LMS, De Schrijver A, De Maagd RA,**
1065 **Kleter GA, Battaglia-De Wilde E** (2022) Occurrence and nature of off-target
1066 modifications by CRISPR-Cas Genome editing in plants. ACS Agric Sci Technol **2**:
1067 192–201.

1068 **Tamura K, Stecher G, Kumar S** (2021) MEGA11: Molecular evolutionary genetics
1069 analysis version 11. Mol Biol Evol **38**: 3022.

1070 **Underwood BA, Tieman DM, Shibuya K, Dexter RJ, Loucas HM, Simkin AJ, Sims**
1071 **CA, Schmelz EA, Klee HJ, Clark DG** (2005) Ethylene-regulated floral volatile
1072 synthesis in petunia corollas. Plant Physiol **138**: 255–266.

1073 **Verdonk JC, Haring MA, Van Tunen AJ, Schuurink RC** (2005) ODORANT1
1074 regulates fragrance biosynthesis in petunia flowers. Plant Cell **17**: 1612–1624.

1075 **de Vetten N, Quattrocchio F, Mol J, Koes R** (1997) The *an11* locus controlling flower
1076 pigmentation in petunia encodes a novel WD-repeat protein conserved in yeast,
1077 plants, and animals. Genes Dev **11**: 1422–1434.

1078 **Wang XC, Wu J, Guan ML, Zhao CH, Geng P, Zhao Q** (2020) Arabidopsis MYB4
1079 plays dual roles in flavonoid biosynthesis. Plant J **101**: 637–652.

1080 **Wiszniewski A, Uberegui E, Messer M, Sultanova G, Borghi M, Duarte GT, Vicente**
1081 **R, Sageman-Furnas K, Fernie AR, Nikoloski Z, et al** (2022) Temperature-
1082 mediated flower size plasticity in Arabidopsis. iScience **25**: 105411.

1083 **Xie P, Shi J, Tang S, Chen C, Khan A, Zhang F, Xiong Y, Li C, He W, Wang G, et**
1084 **al** (2019) Control of bird feeding behavior by Tannin1 through modulating the
1085 biosynthesis of polyphenols and fatty acid-derived volatiles in Sorghum. Mol Plant
1086 **12**: 1315–1324.

1087 **Xu W, Dubos C, Lepiniec L** (2015) Transcriptional control of flavonoid biosynthesis by
1088 MYB-bHLH-WDR complexes. Trends Plant Sci **20**: 176–185.

1089 **Yin R, Messner B, Faus-Kessler T, Hoffmann T, Schwab W, Hajirezaei MR, Von**
1090 **Saint Paul V, Heller W, Schäffner AR** (2012) Feedback inhibition of the general
1091 phenylpropanoid and flavonol biosynthetic pathways upon a compromised flavonol-
1092 3-O-glycosylation. J Exp Bot **63**: 2465–2478.

1093 **Zenoni S, Reale L, Tornielli GB, Lanfaloni L, Porceddu A, Ferrarini A, Moretti C,**
1094 **Zamboni A, Speghini A, Ferranti F, et al** (2004) Downregulation of the *Petunia*
1095 *hybrida α*-Expansin gene *PhEXP1* Reduces the amount of crystalline cellulose in
1096 cell walls and leads to phenotypic changes in petal limbs. Plant Cell **16**: 295–308.

1097 **Zhang H, Koes R, Shang H, Fu Z, Wang L, Dong X, Zhang J, Passeri V, Li Y, Jiang**
1098 **H, et al** (2019) Identification and functional analysis of three new anthocyanin
1099 R2R3-MYB genes in Petunia. Plant Direct **3**: e00114.

1100 **Zhang L, Duan Z, Ma S, Sun S, Sun M, Xiao Y, Ni N, Irfan M, Chen L, Sun Y**
1101 (2023) SlMYB7, an AtMYB4-like R2R3-MYB transcription factor, inhibits
1102 anthocyanin accumulation in *Solanum lycopersicum* fruits. J Agric Food Chem **71**:
1103 18758–18768.

1104 **Zhao J, Zhang W, Zhao Y, Gong X, Guo L, Zhu G, Wang X, Gong Z, Schumaker**
1105 **KS, Guo Y** (2007) SAD2, an importin β-like protein, is required for UV-B response
1106 in Arabidopsis by mediating MYB4 nuclear trafficking. Plant Cell **19**: 3805–3818.

1107 **Zimmermann IM, Heim MA, Weisshaar B, Uhrig JF** (2004) Comprehensive
1108 identification of Arabidopsis thaliana MYB transcription factors interacting with
1109 R/B-like BHLH proteins. Plant J **40**: 22–34.

1110 **Zuker A, Tzfira T, Ben-Meir H, Ovadis M, Shklarman E, Itzhaki H, Forkmann G,**
1111 **Martens S, Neta-Sharir I, Weiss D, et al** (2002) Modification of flower color and
1112 fragrance by antisense suppression of the *flavanone 3-hydroxylase* gene. Mol Breed
1113 **9**: 33–41.

1114 **Zvi MM Ben, Negre-Zakharov F, Masci T, Ovadis M, Shklarman E, Ben-Meir H,**
1115 **Tzfira T, Dudareva N, Vainstein A** (2008) Interlinking showy traits: Co-
1116 engineering of scent and colour biosynthesis in flowers. Plant Biotechnol J **6**: 403–
1117 415.

1118 **Zvi MM Ben, Shklarman E, Masci T, Kalev H, Debener T, Shafir S, Ovadis M,**
1119 **Vainstein A** (2012) PAP1 transcription factor enhances production of
1120 phenylpropanoid and terpenoid scent compounds in rose flowers. New Phytol **195**:
1121 335–345.

1122

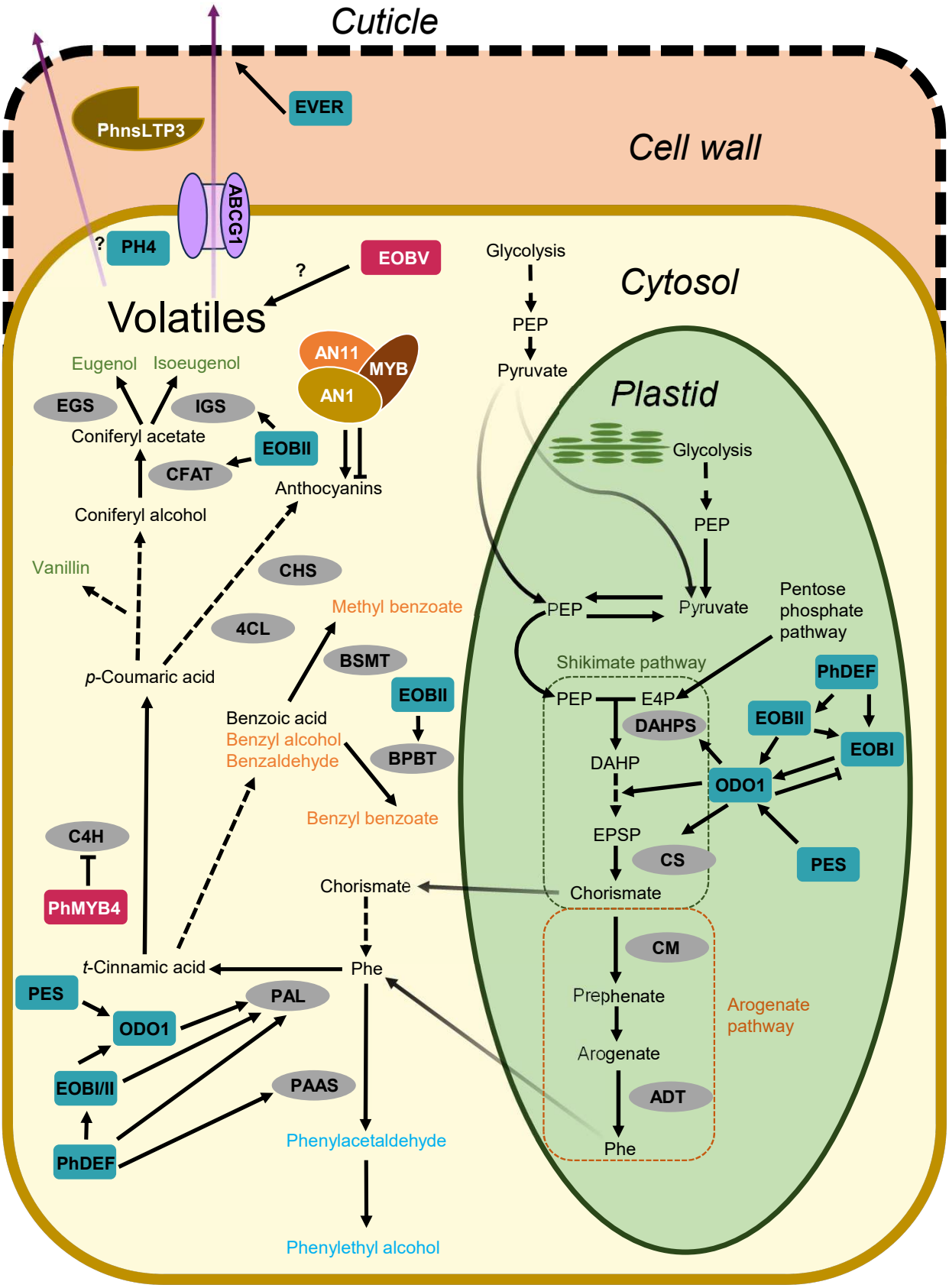
Cuticle
Cell wall
EVER
PhnsLTP3
ABCG1
? PH4
EOBV
?
Volatiles
Cytosol
Glycolysis
PEP
Pyruvate
Plastid
Glycolysis
PEP
Pyruvate
Pentose phosphate pathway
Eugenol
Isoeugenol
EGS
IGS
Coniferyl acetate
EOBII
CFAT
Coniferyl alcohol
AN11
MYB
AN1
Anthocyanins
Vanillin
CHS
4CL
Methyl benzoate
BSMT
p-Coumaric acid
EOBII
Benzoic acid
Benzyl alcohol
Benzaldehyde
BPBT
Benzyl benzoate
Shikimate pathway
PEP
E4P
DAHPS
DAHP
EPSP
CS
Chorismate
PhDEF
EOBII
EOBI
ODO1
PES
C4H
PhMYB4
Chorismate
t-Cinnamic acid
Phe
CM
Prephenate
Arogenate
ADT
Phe
Arogenate pathway
PES
ODO1
PAL
EOBI/II
PhDEF
PAAS
Phenylacetaldehyde
Phenylethyl alcohol

Figure 1 Overview of phenylpropanoid biosynthetic pathways leading to volatile production and emission in petunia flowers. L-phenylalanine (Phe) is synthesized in the plastid or in the cytosol from chorismate generated via the shikimate pathway and arogenate pathways from. From Phe, distinct enzymatic reactions lead to the production of volatiles: benzenoids (C6–C1), shown in orange; phenylpropanoid-related compounds (C6–C2), shown in teal; and phenylpropenes (C6–C3), shown in green. Following their biosynthesis, volatiles are emitted (indicated by purple arrows) across the plasma membrane via the ATP-binding cassette (ABC) transporter PhABCG1 and through the cell wall via the non-specific lipid-transfer protein 3 (PhnsLTP3), before crossing the cuticle. The EPIDERMIS VOLATILE EMISSION REGULATOR (EVER) has been shown to control volatile emission by modulating wax content through the regulation of epicuticular wax biosynthesis. In addition, PH4 has also been shown to affect volatile emission through a yet unknown mechanism. Alternatively, from *p*-Coumaric acid, multiple enzymatic steps lead to the production of anthocyanins, whose biosynthesis is regulated by the MYB–bHLH–WDR (MBW) complex consisting of the bHLH AN1, the WDR protein AN11, and interchangeable MYBs. Enzymes are shown in gray circles; positive and negative transcriptional regulators are shown in teal and red rectangles, respectively. Stacked arrows represent multiple enzymatic steps. Abbreviations: arogenate dehydratase (ADT); benzoyl-CoA:benzylalcohol/2-phenylethanol benzoyltransferase (BPBT); benzoic acid/salicylic acid carboxyl methyltransferase (BSMT); chalcone synthase (CHS); chorismate mutase (CM); chorismate synthase (CS); cinnamate 4-hydroxylase (C4H); coniferyl alcohol acetyltransferase (CFAT); 4-coumarate-CoA ligase (4CL); deficiens (PhDEF); 3-deoxy-D-arabino-heptulosonate-7-phosphate (DAHP); 3-deoxy-D-arabino-heptulosonate-7-phosphate synthase (DAHPS); emission of benzenoids I/II/V (EOBI/II/V); 5-3nolpyruvylshikimate-3-phosphate (EPSP); erythrose-4-phosphate (E4P); eugenol synthase (EGS); isoeugenol synthase (IGS); odorant 1 (ODO1); phenylacetaldehyde synthase (PAAS); L-phenylalanine ammonia-lyase (PAL); phenylpropanoid emission-regulating scarecrow-like (PES); phosphoenolpyruvate (PEP).

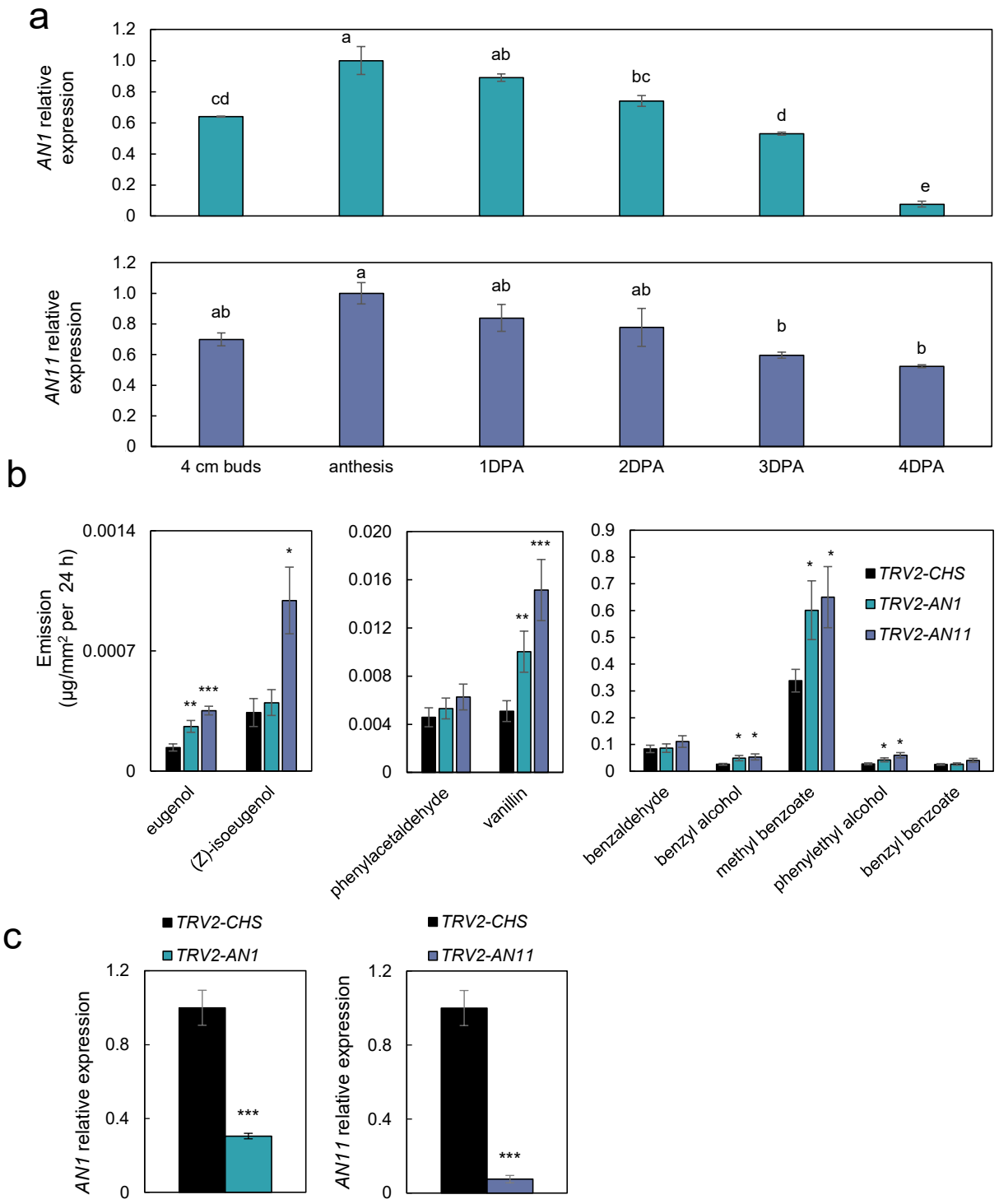

Figure 2 Petunia MBW complex components AN1 and AN11 are involved in negative regulation of volatiles.

a) Developmental expression patterns of *AN1* and *AN11*. RT-qPCR analysis was performed on flower tissues collected at different developmental stages. DPA, days postanthesis. Data are means ± SEM (n = 3). Significance of differences was calculated by Tukey's multiple comparison test following one-way ANOVA. Values with different letters are significantly different at $P \leq 0.05$. **(b and c)** Petunia cv. Mitchell flowers were inoculated at anthesis with agrobacteria carrying pTRV2-AN1, pTRV2-AN11 or pTRV2-CHS as a control. Flowers were harvested 2 days after inoculation and subjected to localized headspace sampling followed by GC–MS analysis **(b)** or RNA extraction followed by RT-qPCR analysis **(c)**. Data are means ± SEM (n = 12). Significance of differences was calculated using Dunnett's test with pTRV2-CHS as the control following one-way ANOVA **(b)** or two-tailed unpaired Student's t-test **(c)** (*$P \leq 0.05$, **$P \leq 0.01$, ***$P \leq 0.001$). **(a and c)** RT-qPCR data were normalized to *ACTIN*, and the presented data were normalized to the sample with the highest expression level. Standard errors are indicated by vertical lines.

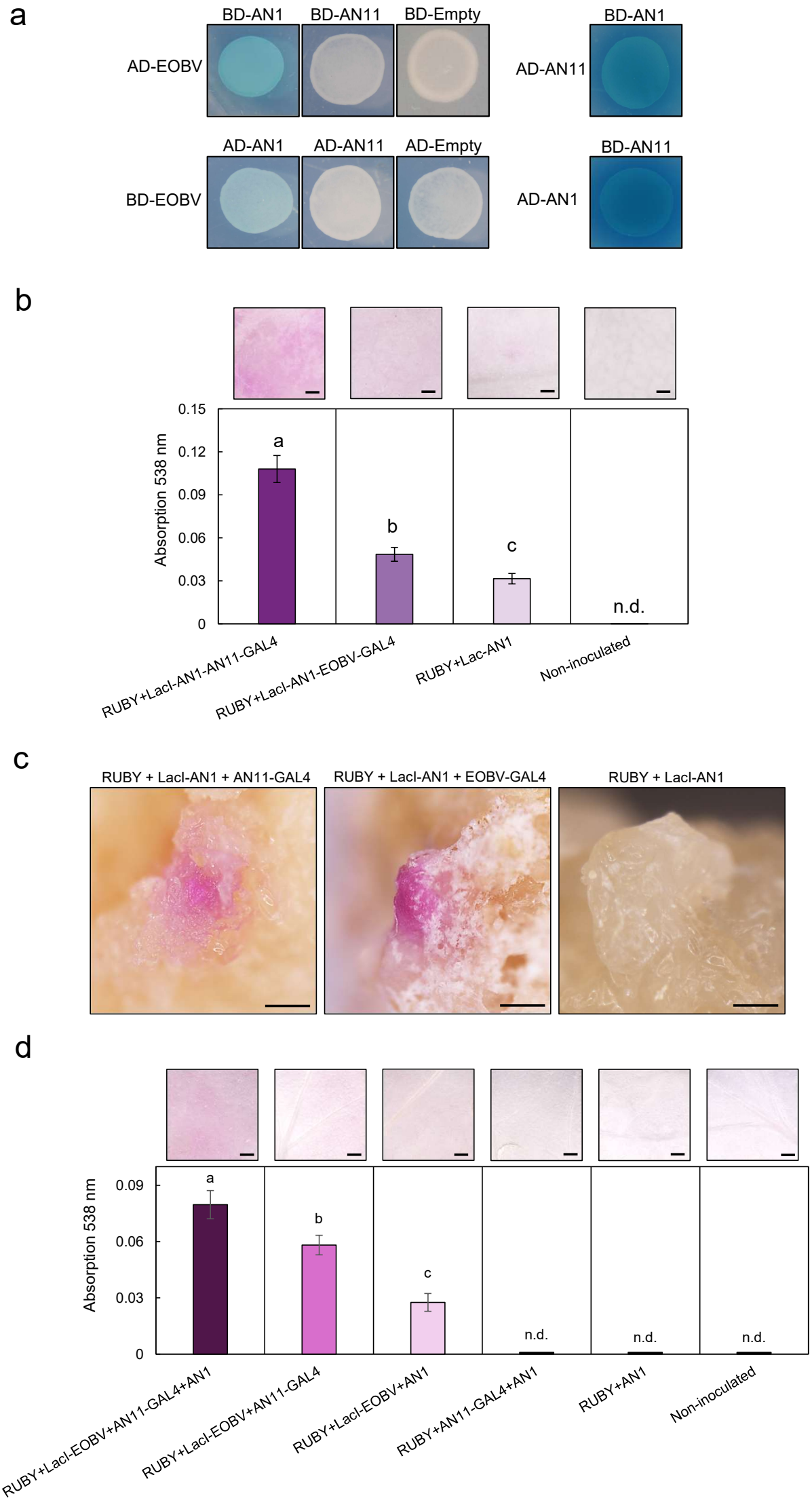
a
BD-AN1
BD-AN11
BD-Empty
AD-EOBV
BD-AN1
AD-AN11
AD-AN1
AD-AN11
AD-Empty
BD-EOBV
BD-AN11
AD-AN1
b
Absorption 538 nm
0.15
0.12
0.09
0.06
0.03
0
a
b
c
n.d.
RUBY+LacI-AN1-AN11-GAL4
RUBY+LacI-AN1-EOBV-GAL4
RUBY+Lac-AN1
Non-inoculated
c
RUBY + LacI-AN1 + AN11-GAL4
RUBY + LacI-AN1 + EOBV-GAL4
RUBY + LacI-AN1
d
Absorption 538 nm
0.09
0.06
0.03
0
a
b
c
n.d.
n.d.
n.d.
RUBY+LacI-EOBV+AN11-GAL4+AN1
RUBY+LacI-EOBV+AN11-GAL4
RUBY+LacI-EOBV+AN1
RUBY+AN11-GAL4+AN1
RUBY+AN1
Non-inoculated

Figure 3 The MYB EOBV is a component of the MBW complex. **a)** Yeast-two hybrid assay was performed by fusing the coding sequences of target proteins to GAL4 binding domain (BD) or GAL4 activation domain (AD), followed by yeast transformation. X-Gal staining was performed on transformed yeast to detect *β*-galactosidase activity, indicating an interaction between bait and prey. The interaction between AN1 and AN11 was used as a positive control (Albert et al., 2014). Vectors without coding sequences (AD:empty, BD:empty) were used as negative controls. **(b–c)** In-planta pairwise protein-interaction assays. **b)** *N. benthamiana* leaves were inoculated with a mixture of agrobacteria carrying the vectors shown in Supplementary Figure 4a; 5 days postinoculation, leaves were harvested and analyzed following immersion in 100% ethanol. Upper panel: representative photos of bleached leaves inoculated with OpLacI:RUBY, 35S:LacI-AN1 and 35S:AN11-GAL4 (positive control); OpLacI:RUBY, 35S:LacI-AN1 and 35S:EOBV-GAL4; OpLacI:RUBY and 35S:LacI-AN1 (negative control); and non-inoculated leaf. Bar = 1 mm. Lower panel: betalain levels in leaves inoculated with the above-described vectors **(c)** Left to right: representative photos of pigmented calli formed on *N. tabacum* leaf disks inoculated with OpLacI:RUBY, 35S:LacI-AN1 and 35S:AN11-GAL4 (positive control); OpLacI:RUBY, 35S:LacI-AN1 and 35S:EOBV-GAL4; OpLacI:RUBY and 35S:LacI-AN1 (negative control). Bar = 0.5 mm. **d)** Three-way in-planta interaction assay. *N. benthamiana* leaves were inoculated with a mixture of agrobacteria carrying the vectors shown in Supplementary Figure 4A and analyzed as described in **(b)**. Upper panel: representative photos of bleached leaves inoculated with OpLacI:RUBY, 35S:LacI-EOBV, 35S:AN11-GAL4 and 35S:AN1; OpLacI:RUBY, 35S:LacI-EOBV and 35S:AN11-GAL4; OpLacI:RUBY, 35S:LacI-EOBV and 35S:AN1; OpLacI:RUBY, 35S:AN11-GAL4 and 35S:AN1; OpLacI:RUBY and 35S:AN1; and non-inoculated leaf. Bar = 1 mm. Lower panel: betalain levels in leaves inoculated with the above-described vectors. Data are means ± SEM (n = 5). Significance of differences was calculated by Tukey's multiple comparison test following one-way ANOVA. Values with different letters are significantly different at $P \leq 0.05$; n.d., not detected. Standard errors are indicated by vertical lines.

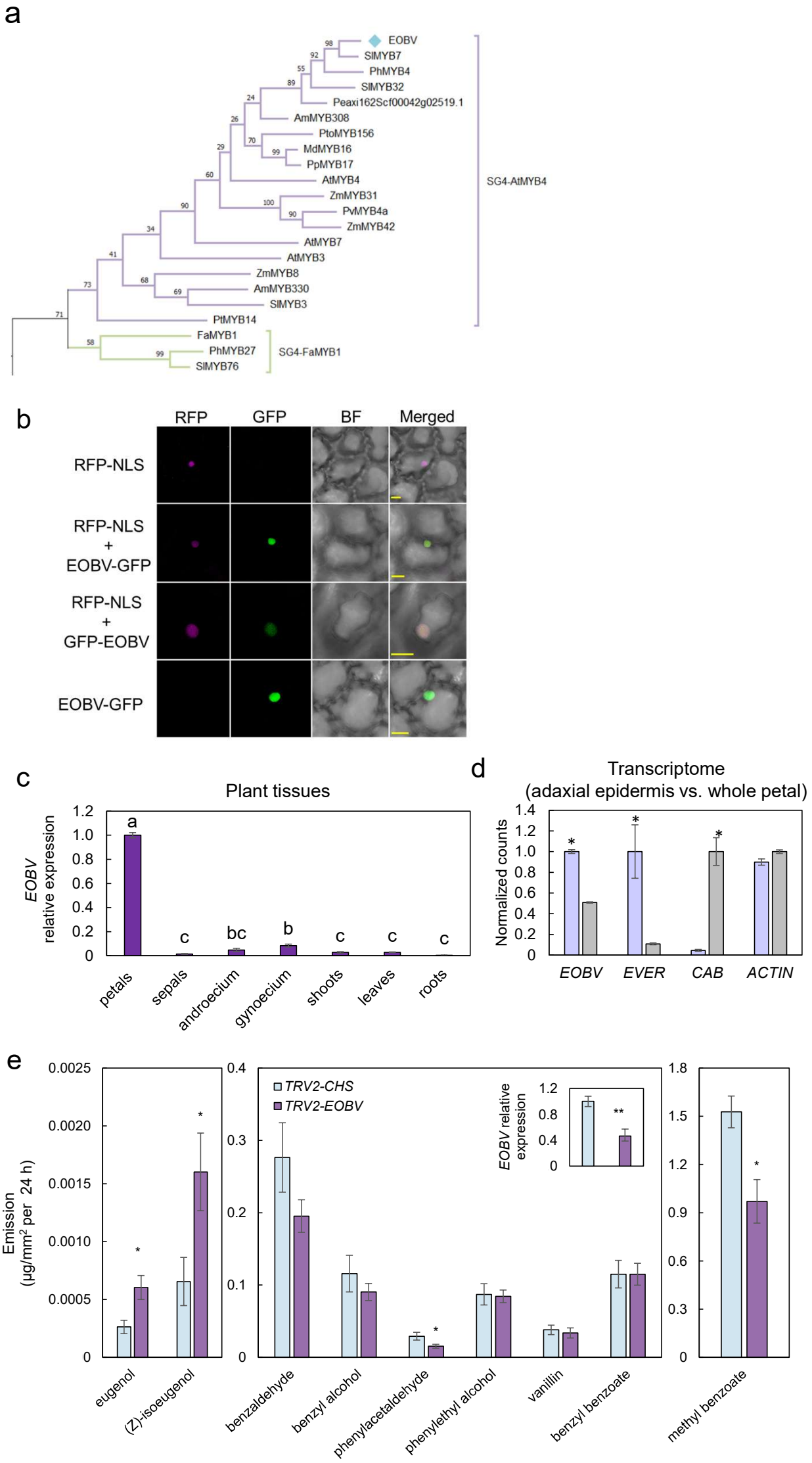
a
EOBV
SlMYB7
PhMYB4
SlMYB32
Peaxi162Scf00042g02519.1
AmMYB308
PtoMYB156
MdMYB16
PpMYB17
AtMYB4
ZmMYB31
PvMYB4a
ZmMYB42
AtMYB7
AtMYB3
ZmMYB8
AmMYB330
SlMYB3
PtMYB14
FaMYB1
PhMYB27
SlMYB76
SG4-AtMYB4
SG4-FaMYB1
b
RFP
GFP
BF
Merged
RFP-NLS
RFP-NLS + EOBV-GFP
RFP-NLS + GFP-EOBV
EOBV-GFP
c
Plant tissues
EOBV relative expression
petals
sepals
androecium
gynoecium
shoots
leaves
roots
d
Transcriptome (adaxial epidermis vs. whole petal)
Nomalized counts
EOBV
EVER
CAB
ACTIN
e
Emission (μg/mm² per 24 h)
TRV2-CHS
TRV2-EOBV
EOBV relative expression
eugenol
(Z)-isoeugenol
benzaldehyde
benzyl alcohol
phenylacetaldehyde
phenylethyl alcohol
vanillin
benzyl benzoate
methyl benzoate

Figure 4 EOBV is a petal epidermis-enriched R2R3-MYB subgroup 4 member that negatively regulates volatiles in petunia flowers. **a)** Phylogenetic tree displaying the similarity between EOBV and subgroup 4 R2R3-MYBs from other plants. Protein sequences were aligned by ClustalW, followed by neighbor-joining method with 1000 bootstraps using MEGA version 11. **b)** Nuclear localization of EOBV in petal epidermal cells by confocal microscopy. Petunia petals were inoculated with agrobacteria carrying *EOBV-GFP* or *GFP-EOBV* and *RFP-NLS,* or only *RFP-NLS* as a control. Bars = 10 µm. BF = bright field. NLS, nuclear localization signal.**c)** Expression of *EOBV* in different plant organs. Tissues from different organs were collected at 1100 h. RT-qPCR data were normalized to *ACTIN*, and the presented data were normalized to the sample with the highest expression level. Significance of differences was calculated by Tukey's multiple comparison test following one-way ANOVA. Values with different letters are significantly different at $P \leq 0.05$. **d)** *EOBV* transcripts are enriched in the petal adaxial epidermis. Normalized counts in the petal adaxial epidermis (purple bars) vs. whole petal (gray bars) based on the transcriptome data from Skaliter *et al*. (2024). Significance of differences was calculated by two-tailed unpaired Student's *t*-test: $^{*}P \leq 0.05$. EVER, EPIDERMIS VOLATILE EMISSION REGULATOR. CAB, CHLOROPHYLL A/B BINDING PROTEIN. **e)** Transient suppression of *EOBV* in petunia cv. Mitchell flowers inoculated with agrobacteria carrying pTRV2-CHS as a control or pTRV2-EOBV. Flowers were harvested 2 days after inoculation and subjected to localized headspace sampling followed by GC–MS analysis or RNA extraction followed by RT-qPCR analysis (inset). Data are means ± SEM (n = 11–12). RT-qPCR data were normalized to *ACTIN*, and the presented data were normalized to those from pTRV2-CHS. Significance of differences between treatments was calculated by two-tailed unpaired Student's *t*-test: ($^{*}P \leq 0.05$, $^{**}P \leq 0.01$, $^{***}P \leq 0.001$). Standard errors are indicated by vertical lines.

a
Target 1
Target 2
Target 3
A
TG
Exon 1
intron
Exon 2
b
pTRV2-sgRNA1-sgRNA2
LB
35S-P
SGP
sgRNA1
sgRNA2
NOS-T
RB
pTRV2-sgRNA1-sgRNA3
sgRNA3
Cas9
110 bp
85 bp
Spacer 1
Spacer 2
Spacer 3
eobv-#1
Δ128 bp
eobv-#2
eobv-#3
c
WT
R2
R/B like
R3
C1
C2
C3
C4
273
eobv-#1
Δ1-42 amino acids
eobv-#2
58
eobv-#3
91
d
Cas9
eobv-#1
eobv-#2
eobv-#3

Figure 5 Generation of *eobv*-knockout lines using a virus-based Cas9 system. **a)** Schematic representation of the genomic sequence of *EOBV* and location of the three Cas9 target sites. **b)** Top: schematic representation of the T-DNA carrying tobacco rattle virus RNA2 (pTRV2) vectors used used for gene editing. SGP, subgenomic promoter; LB, left border; 35S-P, cauliflower mosaic virus 35S promoter; SGP, subgenomic promoter; sgRNA, single guide RNA; NOS-T, nopaline synthase terminator; RB, right border; Cas9, human co-don-optimized *Cas9* gene. Bottom: targeted genomic sequences and Sanger sequencing of *eobv*-knockout lines. Green nucleotides, spacer sequences; red nucleotides, protospacer adjacent motif (PAM). Black arrows mark the predicted cleavage site of Cas9. Magenta box, *EOBV* start codon. **c)** Predicted EOBV protein product in *eobv*-knockout and wild-type (WT) lines. Functional domains are indicated by colored rectangles. Numbers denote amino acid positions. **d)** Representative petunia cv. Mitchell flowers 2 days postanthesis from control *Cas9* and *eobv* lines. Bar = 1 cm.

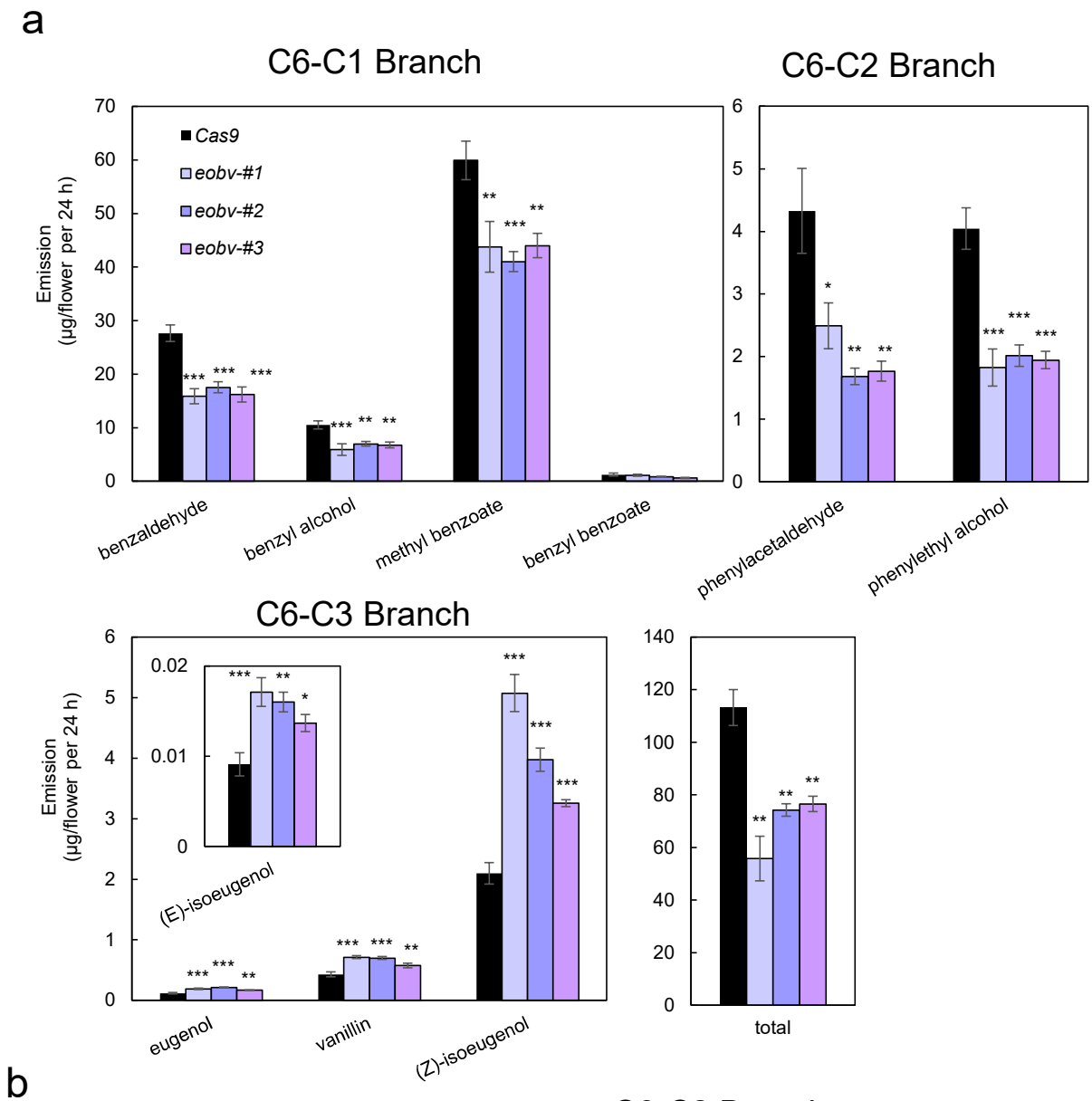
a
C6-C1 Branch
C6-C2 Branch
C6-C3 Branch
Cas9
eobv-#1
eobv-#2
eobv-#3
Emission (µg/flower per 24 h)
benzaldehyde
benzyl alcohol
methyl benzoate
benzyl benzoate
phenylacetaldehyde
phenylethyl alcohol
(E)-isoeugenol
eugenol
vanillin
(Z)-isoeugenol
total

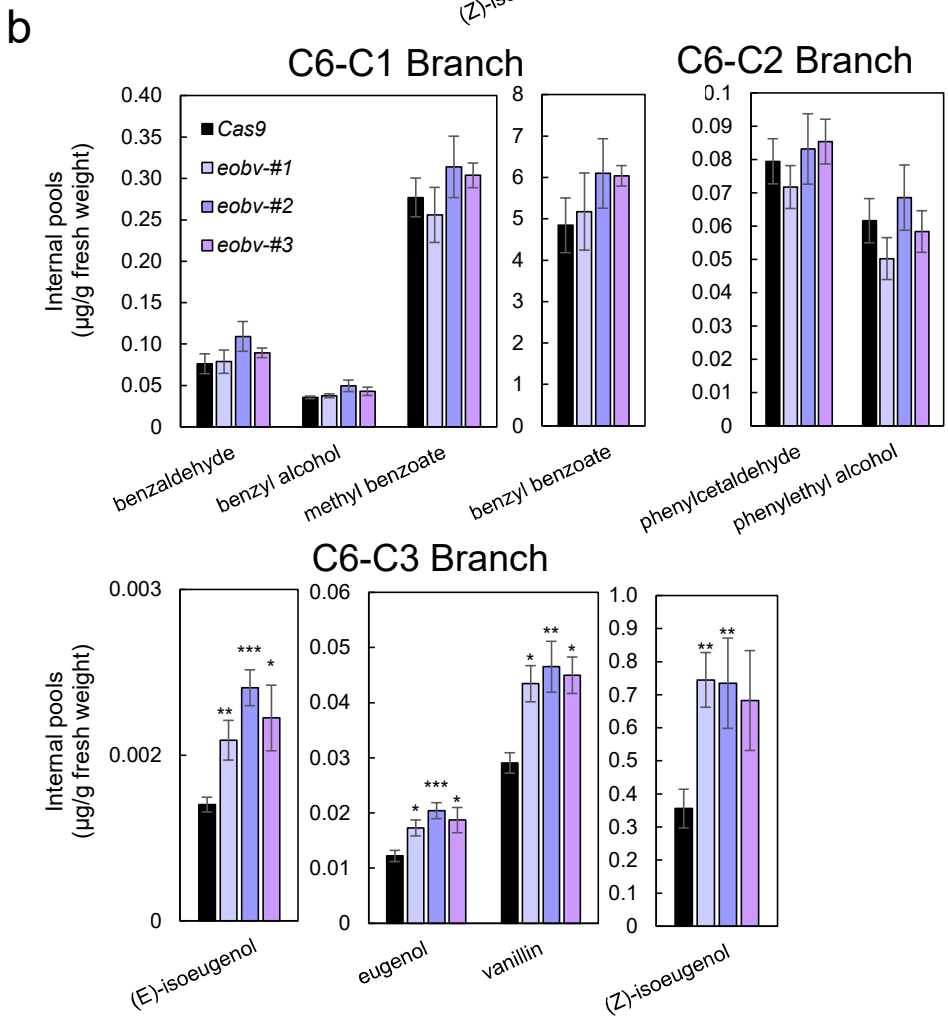
b
C6-C1 Branch
C6-C2 Branch
C6-C3 Branch
Cas9
eobv-#1
eobv-#2
eobv-#3
Internal pools (µg/g fresh weight)
benzaldehyde
benzyl alcohol
methyl benzoate
benzyl benzoate
phenylcetaldehyde
phenylethyl alcohol
(E)-isoeugenol
eugenol
vanillin
(Z)-isoeugenol

Figure 6 *eobv* knockout leads to an increase in phenylpropene production. **a)** Dynamic headspace analyses of *eobv*-knockout lines and *Cas9* control were performed for 24 h on flowers 2 days postanthesis (2DPA) followed by GC–MS analyses. Data are means ± SEM (n = 8–11). **b)** Internal pools were extracted from 2DPA flowers of *Cas9* (control) and *eobv* lines #1–#3 at 2000 h followed by GC–MS analysis. Data are means ± SEM (n = 11–15). Significance of differences was calculated using Dunnett's or Steel's test (*$P \leq 0.05$, **$P \leq 0.01$, ***$P \leq 0.001$) with *Cas9* as the control following one-way ANOVA. Standard errors are indicated by vertical lines.

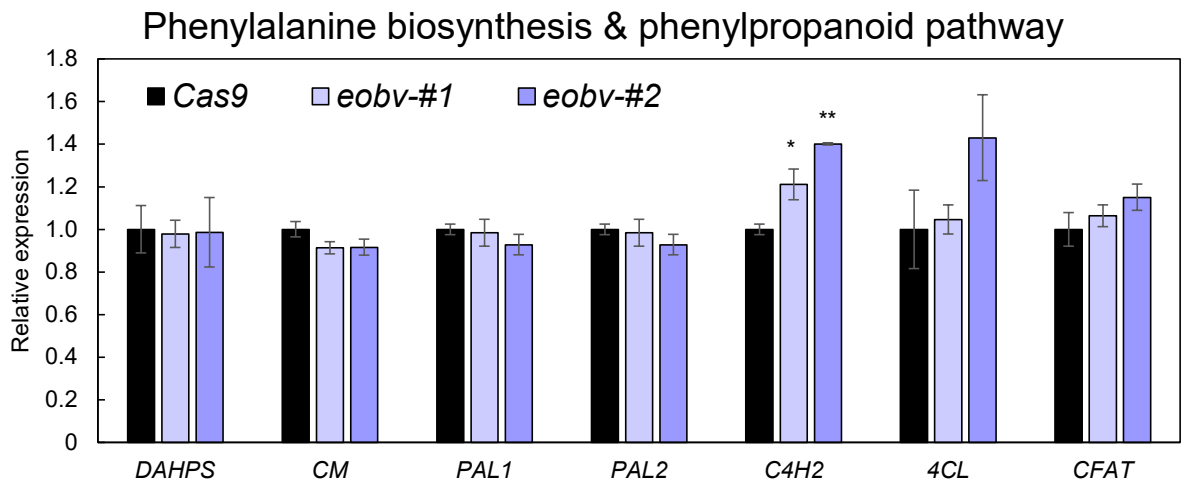
Phenylalanine biosynthesis & phenylpropanoid pathway
Cas9
eobv-#1
eobv-#2
Relative expression
1.8
1.6
1.4
1.2
1.0
0.8
0.6
0.4
0.2
0
*
**
DAHPS
CM
PAL1
PAL2
C4H2
4CL
CFAT

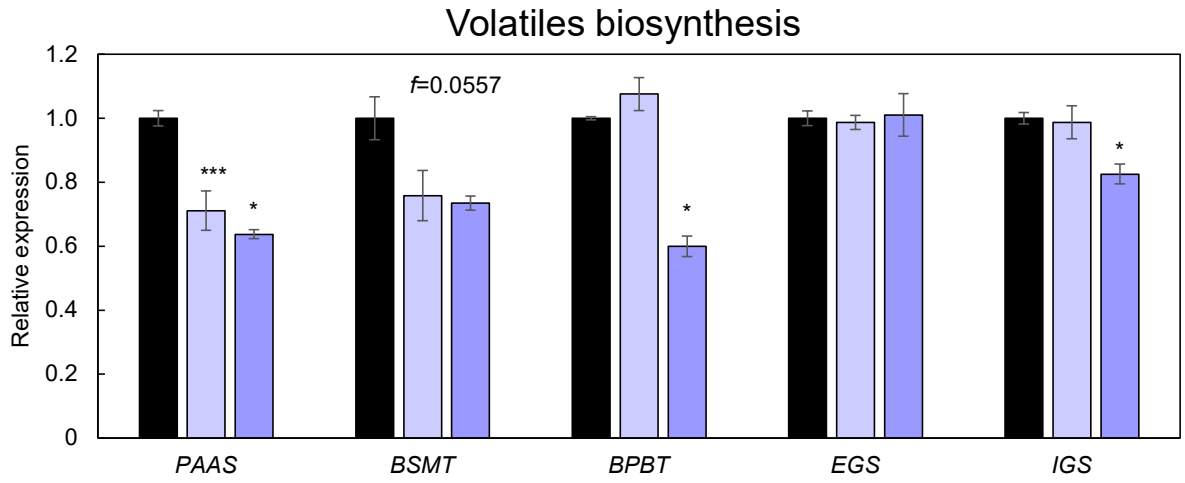
Volatiles biosynthesis
Relative expression
1.2
1.0
0.8
0.6
0.4
0.2
0
f=0.0557
***
*
*
*
PAAS
BSMT
BPBT
EGS
IGS

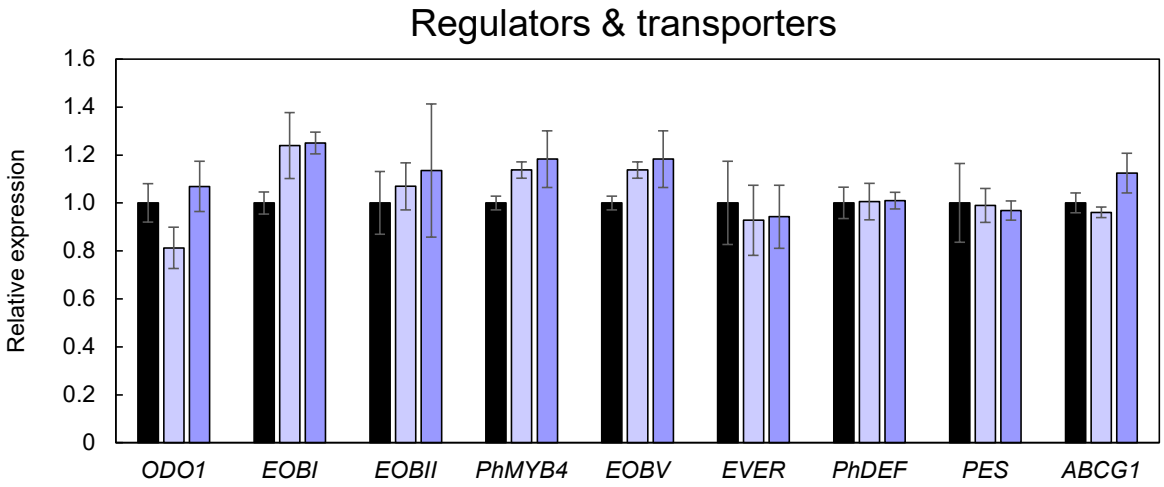
Regulators & transporters
Relative expression
1.6
1.4
1.2
1.0
0.8
0.6
0.4
0.2
0
ODO1
EOBI
EOBII
PhMYB4
EOBV
EVER
PhDEF
PES
ABCG1

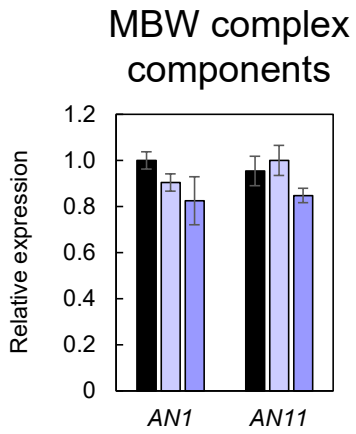
MBW complex components
Relative expression
1.2
1.0
0.8
0.6
0.4
0.2
0
AN1
AN11

Figure 7 *eobv* knockout leads to an increase in *C4H* transcript level. Flowers 2 days postanthesis from *eobv*-knockout lines #1 and #2 and *Cas9* control were harvested at 1900 h and subjected to RT-qPCR analyses. Data are means ± SEM (n = 5). Data were normalized to the geomean of *EF1α* and *ACTIN.* Significance of differences was calculated using Dunnett's or Steel's test (*$P \leq 0.05$, **$P \leq 0.01$, ***$P \leq 0.001$) with *Cas9* as the control following one-way ANOVA. Standard errors are indicated by vertical lines. Phenylalanine biosynthesis and phenylpropanoid pathway genes: DAHPS, ARABINOHEPTULOSONATE 7-PHOSPHATE SYNTHASE; CM, CHORISMATE MUTASE; PAL1, PHENYLALANINE AMMONIA-LYASE 1; PAL2, PHENYLALANINE AMMONIA-LYASE 2; C4H2, CINNAMATE 4-HYDROXYLASE 2; 4CL, 4-COUMARATE:COA LIGASE; CFAT, CONIFERYL ALCOHOL ACYLTRANSFERASE. Volatile biosynthesis genes: PAAS, PHENYLACETALDEHYDE SYNTHASE; BSMT, S-ADENOSYL-L-METHIONINE:BENZOIC ACID/SALICYLIC ACID CARBOXYL METHYLTRANSFERASE; BPBT, BENZOYL-COA:BENZYL ALCOHOL/PHENYLETHANOL BENZOYLTRANSFERASE; EGS, EUGENOL SYNTHASE; IGS, ISOEUGENOL SYNTHASE. Regulator and transporter genes: ODO1, ODORANT1; EOBI, EMISSION OF BENZENOIDS I; EOBII, EMISSION OF BENZENOIDS II; EOBV, EMISSION OF BENZENOIDS V; EVER, EPIDERMIS VOLATILE EMISSION REGULATOR; PhDEF, DEFICIENS; PES, PHENYLPROPANOID EMISSION-REGULATING SCARECROW-LIKE; ABCG1, ATP-BINDING CASSETTE SUBFAMILY G MEMBER 1.

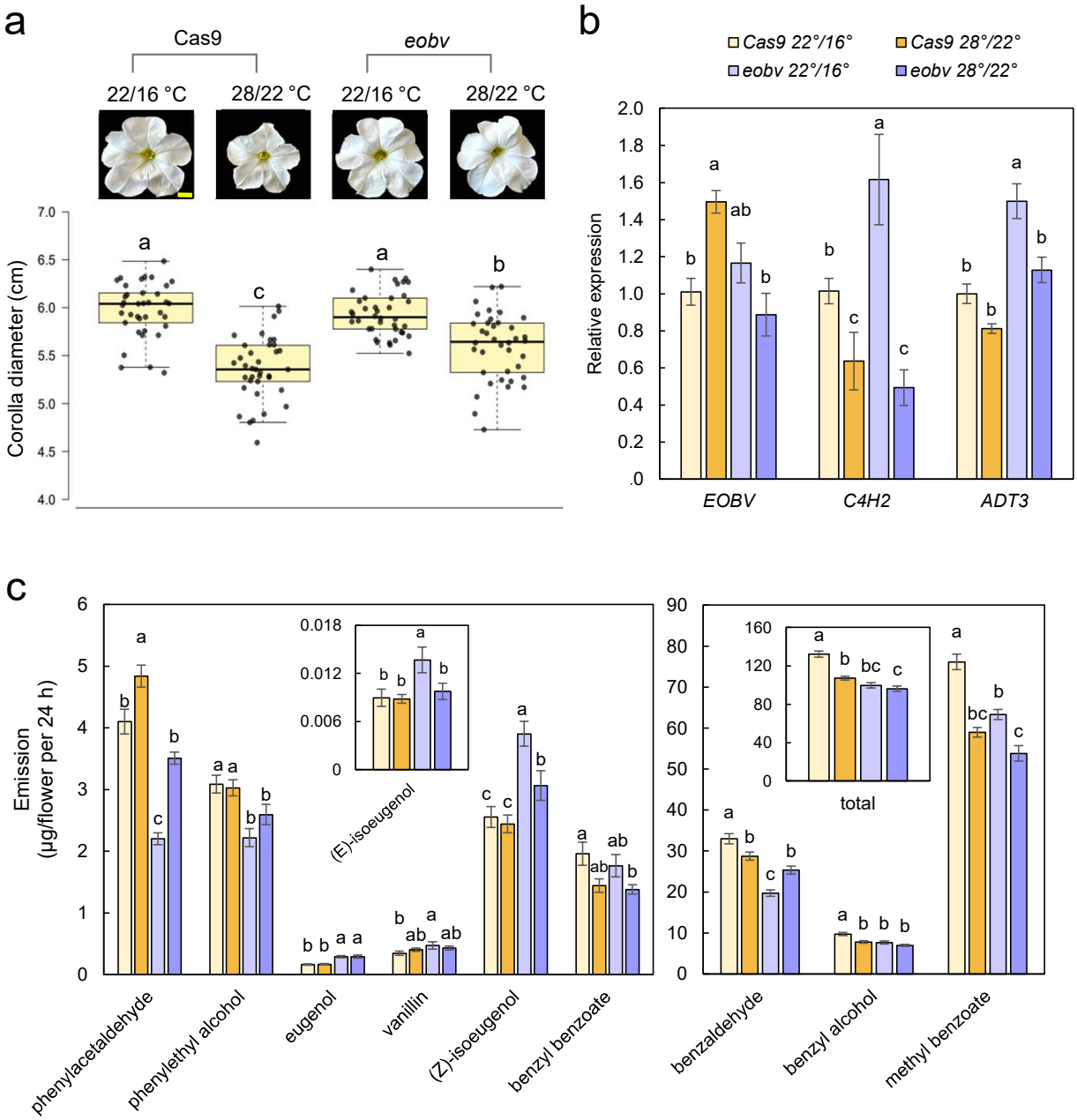

Figure 8 Effect of elevated growth temperature regime on *eobv*-knockout lines. Plants were grown for 1 month in a phytotron at 22/16°C or 28/22°C.
a) Top: representative images of 2 day postanthesis (2DPA) flowers of the different lines and regimes. Bar = 1 cm. Bottom: Diameter of corollas from the different treatments (n = 38). **b)** RT-qPCR analysis of RNA extracted from flowers 2DPA. Data are means ± SEM (n = 5). Data were normalized to the geomean of *EF1α* and *ACTIN*. **c)** Dynamic headspace analysis was performed on flowers 2DPA for 24 h, followed by GC–MS analysis. Data are means ± SEM (n = 10–16). Significance of differences was calculated by Tukey's multiple comparison test following one-way ANOVA. Values with different letters are significantly different at $P \leq 0.05$. Standard errors are indicated by vertical lines. C4H2, CINNAMATE 4-HYDROXYLASE 2; ADT3, AROGENATE DEHYDRATASE 3.